

Closed flux tubes in higher representations and their string description in D=2+1 $SU(N)$ gauge theories

Andreas Athenodorou^a and Michael Teper^b

^aDepartment of Physics, Swansea University, Swansea SA2 8PP, UK

^bRudolf Peierls Centre for Theoretical Physics, University of Oxford,
1 Keble Road, Oxford OX1 3NP, UK

Abstract

We calculate, numerically, the low-lying spectrum of closed confining flux tubes that carry flux in different representations of $SU(N)$. We do so for $SU(6)$ at $\beta = 171$, where the calculated low-energy physics is very close to the continuum limit and, in many respects, also close to $N = \infty$. We focus on the adjoint, 84, 120, $k = 2A, 2S$ and $k = 3A, 3M, 3S$ representations and provide evidence that the corresponding flux tubes, albeit mostly unstable, do in fact exist. We observe that the ground state of a flux tube with momentum along its axis appears to be well defined in all cases and is well described by the Nambu-Goto free string spectrum, all the way down to very small lengths, just as it is for flux tubes carrying fundamental flux. Excited states, however, typically show very much larger deviations from Nambu-Goto than the corresponding excitations of fundamental flux tubes and, indeed, cannot be extracted in many cases. We discuss whether what we are seeing here are separate stringy and massive modes or simply large corrections to energy levels that will become string-like at larger lengths.

E-mail: a.a.athinodorou@swansea.ac.uk, m.teper1@physics.ox.ac.uk

Contents

1	Introduction	1
2	Background and Overview	2
2.1	analytic expectations	3
2.2	fundamental flux tubes	5
2.3	flux tubes in higher representations	5
3	Lattice methods	6
3.1	lattice setup	6
3.2	calculating energies	7
4	Spectrum results	8
4.1	finite volume corrections	9
4.2	$k=2A, 2S$	11
4.3	$k=3A, 3M, 3S$	19
4.4	adjoint	20
4.5	<u>84</u> and <u>120</u>	21
5	Excited states: massive or stringy?	22
6	Discussion and conclusions	25
A	Representations and Casimirs	29

1 Introduction

In the confining phase of $SU(N)$ gauge theories in $3+1$ or $2+1$ dimensions, the flux between sources in the fundamental representation is carried by a flux tube that at large separations, l , will look like a thin string. The spectrum of such a string-like flux tube, whether closed (around a spatial torus) or open (ending at two sources), should be calculable from an effective string action [1, 2] once l is large enough that the energy gap to the ground state has become small compared to the gauge theory's dynamical scale, $\sim O(\Lambda_{\overline{MS}})$ in $D = 3 + 1$ and $\sim O(g^2)$ in $D = 2 + 1$. Indeed, it may be that the spectrum is simple even at smaller l , where the energy gaps are large, once N is so large that flux tubes effectively do not mix or decay. In recent years a great deal of progress has been made in determining the universal terms of this effective string action thus determining the spectrum at large l . (See [3] for a recent review.) Simultaneously, numerical lattice calculations have determined the spectrum at small to medium values of l , where the dynamics turns out to be remarkably close to that of a free string theory (Nambu-Goto in flat space-time).

In this paper we extend our recent lattice calculations of the spectrum of closed flux tubes in $2+1$ dimensions [6] to the case where the flux is in representations other than the

fundamental. This will include cases where the flux tube is stable for all l (e.g. the ground states of \mathcal{N} -ality $k = 2$ or $k = 3$) and cases where it is not. Whether the latter do have a well-defined identity is an interesting question which we shall also address, albeit only empirically in this paper. (We are not aware of a quantitative theoretical analysis of the binding and decay of such ‘composite’ flux tubes, although the general framework for decays has been developed in [4], and it would be interesting to understand if the flux tubes considered in this paper satisfy the conditions for those calculations to be accurate. See also [5] for related work.) As in our earlier work [6] nearly all our calculations are in SU(6), where the theory is close to its $N = \infty$ limit for many low-energy quantities, but far enough away from that limit for the $k = 2$ and $k = 3$ ground states to be well below their decay thresholds. Our calculations are at a fixed value of the lattice spacing a that is small enough for most lattice corrections to be negligible (within our statistical accuracy).

In the next Section we provide a (very) brief sketch of relevant analytic and numerical results. We then describe the technical aspects of the lattice calculation. In Section 4 we present our results. We begin with flux tubes carrying flux in the $k = 2$ symmetric and anti-symmetric representations (that arise from $f \otimes f$, where f is the fundamental representation), then move on to the three minimal $k = 3$ representations (arising from $f \otimes f \otimes f$), the adjoint flux tube (from $f \otimes \bar{f}$) and those carrying flux in the 84 and 120 representations (arising from $f \otimes f \otimes \bar{f}$). The Appendix describes the properties of these representations. Such flux tubes, when they exist, can be thought of as bound states of (anti)fundamental flux tubes and their spectra should contain the imprint of the massive modes associated with that binding. The latter should be additional to the usual massless stringy modes, which are the only ones to appear in the spectrum of fundamental flux tubes in $D = 2 + 1$ [6].

The lattice calculations are very similar to our earlier work with fundamental flux and we refer to that work [6] for most of the technical details. We also note our earlier calculation of the spectrum of $k = 2$ flux tubes [7] performed at smaller N and for coarser a , and to earlier calculations of k -string tensions [8]. We refer to these for a more detailed discussion of k -strings.

2 Background and Overview

We are interested in the spectrum of flux tubes that are closed around a spatial torus of length l . We make the sizes of the transverse spatial torus, l_\perp , and the (Euclidean) temporal torus, l_t , large enough that the resulting finite size corrections are negligible. As l decreases, the theory suffers a finite volume transition at $l = l_c = 1/T_c$ where T_c is the deconfining temperature, and for $l \leq l_c$ the theory does not support winding flux tubes. This transition is strongly first order for SU(6), the case of interest in this paper. Since $T_c \sim \sqrt{\sigma_f}$ in terms of the fundamental string tension, this means we can study closed flux tubes of length $l \gtrsim 1/\sqrt{\sigma_f}$.

Since the spectrum of the Nambu-Goto model turns out to be an excellent starting point for much of the observed fundamental flux tube spectrum, we begin by briefly summarising it. We then say something about relevant analytic results for long flux tubes – an area in which striking progress has been made in the last few years – as well as the numerical results

for flux tubes in the fundamental representation, which the present work extends to higher representations. We then say something about those higher representations.

2.1 analytic expectations

Recall that we consider flux tubes that are closed around a spatial torus of length l , with the transverse and Euclidean time tori chosen so large as to be effectively infinite. Such flux tubes may carry non-zero longitudinal momentum. (We do not consider non-zero momentum transverse to the string since that does not teach us anything new.) In the $N \rightarrow \infty$ limit where decays and mixings are suppressed, the world sheet swept out by the propagating flux tube has no handles or branchings and so has the simple topology of a cylinder. The simplest effective string action is proportional to the invariant area of the sheet in flat space-time (Nambu-Goto). The Nambu-Goto spectrum arises from left and right moving massless ‘phonons’ on the background string of tension σ . Let $n_{L(R)}(k)$ be the number of left(right) moving phonons of momentum $|p| = 2\pi k/l$ and define their total energy to be $2\pi N_{L(R)}/l$, i.e.

$$N_L = \sum_k n_L(k)k, \quad N_R = \sum_k n_R(k)k. \quad (1)$$

so that the state has total longitudinal momentum $p = 2\pi q/l$ with

$$N_L - N_R = q. \quad (2)$$

The energy levels in $D = 2 + 1$ turn out to be given by [9, 10]

$$E_n(q, l) = \left\{ (\sigma l)^2 + 8\pi\sigma \left(\frac{N_L + N_R}{2} - \frac{1}{24} \right) + \left(\frac{2\pi q}{l} \right)^2 \right\}^{\frac{1}{2}} \quad (3)$$

where $n = N_L + N_R$ and one can readily calculate the degeneracy of a given energy level. We note that the parity of a state is given by

$$P = (-1)^{\text{number of phonons}}. \quad (4)$$

We display in Table 1 the states which we will later discuss in more detail. (Here $a_{\pm k}$ creates a phonon of momentum $\pm 2\pi k/l$.) We refer to [6] for a more detailed discussion, and reasons why we ignore quantum numbers other than parity and momentum along the flux tube.

Note that the spectrum in eqn(3) is derived using naive light-cone quantisation [9]. Its actual relationship with Nambu-Goto in $D < 26$ is a subtle question, which is considered critically in [3]. We will nonetheless use it for comparative purposes and refer to it as ‘the Nambu-Goto spectrum’.

For large enough l we can expand eqn(3) in powers of $1/\sigma l^2$. The first correction to the linear σl piece coincides with the well-known $O(1/l)$ universal Lüscher correction [1, 2]. It is now known that the $O(1/l^3)$ correction is also universal [10, 11] as is the $O(1/l^5)$ correction [12]. (This is for $D = 2 + 1$; there are interesting differences in $D = 3 + 1$ [3]). The universality

N_L, N_R	q	P	String State
$N_L = 0, N_R = 0$	0	+	$ 0\rangle$
$N_L = 1, N_R = 0$	1	−	$a_1 0\rangle$
$N_L = 1, N_R = 1$	0	+	$a_1 a_{-1} 0\rangle$
$N_L = 2, N_R = 0$	2	+	$a_1 a_1 0\rangle$
		−	$a_2 0\rangle$
$N_L = 2, N_R = 1$	1	+	$a_2 a_{-1} 0\rangle$
		−	$a_1 a_1 a_{-1} 0\rangle$
$N_L = 2, N_R = 2$	0	+	$a_2 a_{-2} 0\rangle$
		+	$a_1 a_1 a_{-1} a_{-1} 0\rangle$
		−	$a_2 a_{-1} a_{-1} 0\rangle$
		−	$a_1 a_1 a_{-2} 0\rangle$
$N_L = 3, N_R = 3$	0	+	$a_3 a_{-3} 0\rangle$
		+	$a_2 a_1 a_{-2} a_{-1} 0\rangle$
		+	$a_1 a_1 a_1 a_{-1} a_{-1} a_{-1} 0\rangle$
		+	$a_1 a_1 a_1 a_{-3} 0\rangle$
		+	$a_3 a_{-1} a_{-1} a_{-1} 0\rangle$
		−	$a_3 a_{-2} a_{-1} 0\rangle$
		−	$a_2 a_1 a_{-3} 0\rangle$
		−	$a_2 a_1 a_{-1} a_{-1} a_{-1} 0\rangle$
		−	$a_1 a_1 a_1 a_{-2} a_{-1} 0\rangle$

Table 1: The states of the lowest Nambu-Goto energy levels with $p = 2\pi q/l$ for $q = 0, 1, 2$, and $q = 0$ excited states with $N_L + N_R \leq 6$.

class is determined by the massless modes living on the string. If, as is plausible here, the only such modes are those arising from the bosonic massless transverse oscillations, then these universal terms coincide with the corresponding terms in the expansion of the Nambu-Goto action and energy levels [12, 13]. Thus once l is large enough for the expansion of eqn(3) in powers of $1/l^2\sigma$ to converge (which occurs at small l only for the absolute ground state) we can expect the free string Nambu-Goto theory to provide an increasingly accurate description of that part of the closed flux tube spectrum.

Note that such effective string calculations become valid for an excited flux tube once l becomes large enough that the energy gap $\Delta E_n \simeq E_n(l) - \sigma l$ becomes small compared to the dynamical energy scale of the theory $\sim \sqrt{\sigma}$. And this is so independent of N . However the expansion of eqn(3) only requires $\Delta E_n \lesssim \sigma l$ which is a weaker condition. So for the effective string approach to be valid all the way down to the Nambu-Goto radius of convergence we presumably need to invoke nearness to the $N = \infty$ limit as well.

While the above analytic progress has so far concerned flux tubes at large enough l , we remark that there have been promising recent attempts at understanding the spectrum at smaller l from considerations of the scattering matrix of phonons on the world sheet [14]. (See also [15].)

These analytic results assume that the flux is carried by a single flux tube. While this

is indeed the case for fundamental flux tubes, in appropriate limits, it is not clear what happens for higher representations R . While we can still expect an effective (Goldstone) action approach to be valid as long as $\Delta E_n \simeq E_n(l) - \sigma_R l < \sqrt{\sigma_f}$, extending the range of validity by an appeal to large N is dubious. Indeed, in the $N = \infty$ limit we expect the flux to be carried by an appropriate number of non-interacting fundamental flux tubes. (As we shall see below when we consider explicit operators for such flux.) Thus we are not able to rely on an ideal $N \rightarrow \infty$ limit in the same way as we can for fundamental flux tubes.

2.2 fundamental flux tubes

In [6] we performed calculations in SU(6) of the closed flux tube spectrum on the same lattices, and at the same coupling as in this paper. We briefly list some of the conclusions of that work that are relevant to this paper.

- 1) The absolute ground state is very accurately described by the free string prediction in eqn(3), with a correction only becoming visible for $l\sqrt{\sigma_f} \lesssim 2$.
- 2) This correction is consistent, within the errors, with being either $\propto 1/l^5$ or $\propto 1/l^7$, where the latter is the prediction of the analysis of universal terms.
- 3) The lightest states with $p \neq 0$ also show no visible correction to Nambu-Goto down to $l\sqrt{\sigma_f} \sim 1.5$. These states contain phonon excitations and so we see that the flux tube behaves like an excited thin string even when its length is about the same as its width (which is naively $\sim \sqrt{\sigma_f}$).
- 4) In general whenever an excited state corresponds to phonons that are all right or left moving, corrections to Nambu-Goto are almost invisible.
- 5) While other low-lying excited states typically show larger corrections, these typically become insignificant at values of l that are much smaller than required for the expansion of eqn(3) in powers of $1/l^2\sigma$ to become convergent. That is to say, our results show that the Nambu-Goto prediction is still good when all the terms in the $1/l^2\sigma$ expansion are important: i.e. the series of correction terms must itself resum to a modest total correction even at small l .
- 6) There is no evidence at all of any non-stringy massive modes that are additional to the stringy ones that are well described by the free string theory spectrum.

One of our main motivations for the present study is to contrast the above with what one finds for flux tubes that are bound states of fundamental flux tubes, and where the binding, measurable through the value of the string tension, provides unambiguous massive dynamics that should somehow make itself seen in the flux tube spectrum.

2.3 flux tubes in higher representations

Consider two well separated sources in representations R and \bar{R} . The flux between them will be carried by one or more confining flux tubes and, if we ignore the possibility of screening, will be in the representation R .

The representations of SU(6) that we consider in this paper are the fundamental f , the adjoint A which appears in $f \otimes \bar{f}$, the representations 84 and 120 which appear in $f \otimes f \otimes \bar{f}$,

and the various irreducible representations generated by $f \otimes f$ and $f \otimes f \otimes f$. These last two belong to the $k = 2$ and $k = 3$ sectors respectively. That is to say under a global gauge transformation that is an element of the centre, $g(x) = e^{i\pi/N}\mathbb{I}$, the sources transform as $= e^{i\pi k/N}$. Under this categorisation the f , 84 and 120 belong to $k = 1$ and the adjoint A to $k = 0$. In the $k = 2$ sector we consider the antisymmetric $2A$ and symmetric $2S$ representations. In the $k = 3$ sector we consider the antisymmetric $3A$, the mixed $3M$, and the symmetric $3S$ representations. All these representations are discussed in more detail in the Appendix.

Since gluons transform trivially under the centre, screening cannot change the value of k . Hence the absolute ground state in each k -sector will correspond to an absolutely stable flux tube. These are often referred to as k -strings, although this term is often used more loosely to label all states in a given k -sector. Note that there will be an absolutely stable ground state for each parity, P , and longitudinal momentum, p , within each k -sector. (Note also that at a given l the lightest state with such non-trivial quantum numbers may include a glueball that carries some of the quantum numbers. Such states decouple from our calculations in the $N \rightarrow \infty$ limit and, as we shall see, appear to play no role even for $N = 6$.)

Earlier work [16, 17, 7] has shown that the $k = 2, 3$ ground states are almost exactly $2A$ and $3A$ respectively, except when the flux tube is very short, $l \sim l_c$. This is related to the observation that, despite the fact that gluon screening can take one from e.g. $2S$ to $2A$, the actual overlap is found to be extremely small [8]. This interesting feature of the dynamics is something we shall examine in more detail in this paper.

We note that some overlaps are lower order in $1/N$ and hence would be naturally suppressed for $SU(6)$. This includes the overlap of the adjoint flux tube to the vacuum (or glueballs) and the 84 and 120 flux tubes to a single fundamental, f , flux tube. On the other hand the overlap of the adjoint onto a pair of flux tubes, one f and the other \bar{f} , should not be suppressed. Similarly for 84 and 120 to three flux tubes, 2 f s and one \bar{f} . We will be careful to discuss these possibilities when we present our results below.

3 Lattice methods

3.1 lattice setup

Our space-time is a periodic cubic $L_x \times L_y \times L_t$ lattice with lattice spacing a . The degrees of freedom are $SU(N)$ matrices, $U_\mu(x, y, t)$ or more compactly U_l , assigned to the links l of the lattice. The action is the standard Wilson plaquette action, so the partition function is

$$Z(\beta) = \int \prod_l dU_l e^{-\beta \sum_p \{1 - \frac{1}{N} \text{ReTr} U_p\}} \quad (5)$$

where U_p is the ordered product of matrices around the boundary of the elementary square (plaquette) labelled by p . Taking the continuum limit, one finds that

$$\beta \stackrel{a \rightarrow 0}{\simeq} \frac{2N}{ag^2} \quad (6)$$

where g^2 is the coupling and ag^2 is the dimensionless coupling on the length scale a . The continuum limit is approached by tuning $\beta = 2N/ag^2 \rightarrow \infty$.

3.2 calculating energies

Here we give a brief sketch and refer the reader to Section 3 of [6] for a detailed exposition.

We calculate energies from the time behaviour of correlators of suitable operators $\{\phi_i\}$,

$$C_{ij}(t) = \langle \phi_i^\dagger(t) \phi_j(0) \rangle = \langle \phi_i^\dagger e^{-H a n_t} \phi_j \rangle = \sum_k c_{ik} c_{jk}^* e^{-a E_k n_t}. \quad (7)$$

Since we wish to project onto loops of flux closed around the x -torus, we use operators that wind around the x -torus. The simplest such operator is the Polyakov loop

$$l_p(n_y, n_t) = \prod_{n_x=1}^{L_x} U_x(n_x, n_y, n_t) \quad ; \quad \phi(n_y, n_t) = \text{Tr}_R \{ l_p(n_y, n_t) \} \quad (8)$$

where $l = aL_x$ (we shall measure l in physical units and L in lattice units, unless indicated otherwise) and we have taken the product of the link matrices in the x -direction, around the x -torus and the trace is taken in the desired representation R . We also use many other winding paths, as listed in Table 2 of [6], and also with smeared and blocked $SU(N)$ link matrices [6]. Using all these paths we can project onto different longitudinal momenta and parities. The transverse momentum dependence is determined by Lorentz invariance and so we only consider $p_\perp = 0$ operators, obtained by summing over spatial sites, e.g. $l_p(p_\perp = 0, n_t) \propto \sum_{n_y} l_p(n_y, n_t)$ in eqn(8). Unless otherwise stated all winding operators in this paper will be with $p_\perp = 0$.

We now perform a variational calculation of the spectrum, maximising $\langle e^{-Ht} \rangle$ over this basis (usually projected onto the desired quantum numbers). We usually do so for $t = a$ and this provides us with an ordered set of approximate energy eigenoperators $\{\psi_i\}$. We then form the correlators of these, $\langle \psi_i^\dagger(t) \psi_i(0) \rangle$, and extract the energies from plateaux in the effective energies, defined by

$$\frac{\langle \psi_i^\dagger(t) \psi_i(0) \rangle}{\langle \psi_i^\dagger(t-a) \psi_i(0) \rangle} = \exp\{-a E_{i,eff}(t)\}. \quad (9)$$

These plateaux typically begin at values of t that are larger than $t = a$. Given the propagation of statistical errors, we can only identify such a plateau if it corresponds to the operator having a large overlap onto the desired state. Note that this largely excludes the possibility that our energy estimate is contaminated by a small admixture of a lower lying state. (The effective energy only provides an upper bound on the desired energy if extracted where we perform the variational calculation, i.e. $t = a$ in our case.) It is only where we have significant evidence for a plateau that we quote an energy.

This above procedure is appropriate for stable states. However many of our states will be unstable. (We will usually indicate that in our figures.) If these states are analogous to narrow resonances then they are just as relevant to us as they would be if stable. If the decay width is very small (as it often might be because N is quite large) then by continuity

Rep	$a^2\sigma_R$	σ_R/σ_f	C_R/C_f
f	0.007365(7)	—	—
2A	0.011980(30)	1.627(5)	1.6
2S	0.016536(70)	2.245(10)	2.286
3A	0.013571(50)	1.842(8)	1.8
3M	0.02101(14)	2.853(20)	2.829
3S	0.02799(21)	3.800(30)	3.857
adj	0.015072(75)	2.046(11)	2.057
84	0.020212(81)	2.744(12)	2.714
120	0.02458(22)	3.337(30)	3.4

Table 2: String tensions for various representations (see text) in SU(6) at $\beta = 171$. Also ratios to the fundamental and predictions of Casimir scaling.

we expect that within our finite errors the correlators will behave just as they do for stable states. Conversely, if our correlator looks just like that of a stable state, with an apparently well-defined energy plateau, we can assume that the state is very narrow, and extract an energy. This will certainly not always be the case. Sometimes we have accurate correlators out to large n_t where there is no sign of a plateau, presumably because the state has a large decay width. We shall perform a heuristic analysis of some of these cases when we come to them. The interesting conclusion will be that this leads to an energy much higher than one would naively guess by looking at the effective energies.

We remark that the exact eigenstates of H consist of asymptotic states composed of any stable flux tubes and scattering states of these. (And in addition, at finite N , of stable glueballs.) In particular this includes scattering states of fundamental and antifundamental flux tubes with various relative momenta. However our basis of operators will usually (although not intentionally) have a small overlap on these, and so we usually will not see them in our calculation. We will comment further on this when we consider examples of what are presumably unstable states.

4 Spectrum results

In this section we present our results. Before entering into details we list in Table 2 the string tension σ_R that we obtain by fitting the absolute ground state energy, $E_0(l)$, for each representation with the Nambu-Goto expression in eqn(10) plus a $O(1/l^7)$ correction, i.e.

$$E_0(l) = \sigma l \left\{ 1 - \frac{\pi}{3} \frac{1}{\sigma l^2} \right\}^{\frac{1}{2}} + \frac{c}{l^7} \quad (10)$$

We use this correction because it is the leading correction to the universal terms [3], but since any correction will only affect $E_0(l)$ at small l our particular choice does not affect the value of the extracted string tension. We compare the ratio σ_R/σ_f to the ratio of the quadratic

		$aE(l)$					
l	$l_{\perp} \times l_t$	f	2A	2S	3A	3M	3S
16	100×200	0.0777(3)	0.1460(14)	0.2256(29)	0.1742(11)	0.2705(61)	0.395(10)
20	70×120	0.1176(5)	0.2088(17)	0.2955(57)	0.2433(21)	0.3723(99)	0.529(10)
24	48×60	0.1528(9)	0.2649(23)	0.3669(42)	0.3020(32)	0.4593(80)	0.651(12)
28	48×60	0.1842(8)	0.3198(29)	0.4490(53)	0.3569(39)	0.5720(86)	0.781(15)
32	40×48	0.2177(10)	0.3633(22)	0.5067(68)	0.4198(53)	0.6304(107)	0.855(15)
36	40×48	0.2490(12)	0.4192(25)	0.5777(70)	0.4762(50)	0.7411(126)	0.963(25)
40	48×48	0.2817(14)	0.4615(42)	0.6504(82)	0.5259(67)	0.8173(123)	1.154(30)
44	48×48	0.3113(14)	0.5144(50)	0.7094(132)	0.5806(74)	0.9102(165)	1.219(49)
48	48×48	0.3425(13)	0.5624(40)	0.7818(96)	0.6405(79)	1.0101(197)	–
52	52×52	0.3723(10)	0.6183(60)	0.8736(104)	0.7015(83)	1.1125(300)	1.473(34)
64	64×64	0.4637(17)	0.7661(109)	1.0789(229)	0.8633(139)	1.3518(194)	1.837(73)

Table 3: The energies, $E(l)$, of the lightest flux tubes of length l (all l in lattice units) and $p = 0$, and with the flux belonging to the indicated representations. The fundamental (f) values are from [6]. For SU(6) at $\beta = 171.0$.

Casimirs, C_R/C_f . There are old arguments for such ‘Casimir scaling’ (see [16] for a discussion and references) as well as newer ones, e.g. [18]. We see from Table 2 that it works remarkably well. This corroborates earlier studies [17, 8] for some of these representations. (As well as older studies in SU(3) of open flux tubes, e.g. [19].) The values of $E_0(l)$ that go into these fits are listed in Tables 3 and 4 where we also show the lattice sizes used. For completeness we include the values for the fundamental representation obtained in our earlier work [6].

4.1 finite volume corrections

Calculations on $l \times l_{\perp} \times l_t$ lattices will suffer finite volume corrections if l_{\perp} and l_t are not large enough. This problem becomes more severe as l decreases. Some checks have been performed in [21, 7] for $k = 2$ flux tubes, and in [6] for excited states of $k = 1$ flux tubes. Since our calculations are now more accurate, it is worth revisiting this question.

We focus on our shortest flux tube, where we employ a $16 \times 100 \times 200$ lattice. We are confident that $l_t/a = 200$ is long enough since $e^{-El_t} = e^{-200aE(l=16)}$ is negligible for all the $l/a = 16$ flux tube energies listed in Tables 3 and 4. We therefore test whether $l_{\perp}/a = 100$ is large enough and we do this by performing calculations on $16 \times l_{\perp}/a \times 200$ lattices with $l_{\perp}/a = 20, 40, 60, 80$. To speed up these very slow calculations we use a much reduced basis of operators - just the simplest Polyakov loops at various blocking levels. This still allows us to obtain accurate values for the ground states but not for any of the excited states. (Which is why we introduced our extended operator basis in the first place.) So for the excited states we continue to rely on the study in [6] and the rescaling of those results to our lattice spacing.

In Table 5 we show our results for the ground states in various representations. We see that the fundamental flux tube suffers no finite volume corrections for $l_{\perp}/a \geq 40$ within the

$aE(l)$				
l	$l_{\perp} \times l_t$	<u>84</u>	<u>120</u>	adj
16	100×200	–	–	0.1658(66)
20	70×120	0.3658(35)	0.4460(47)	0.2568(70)
24	48×60	0.4476(55)	0.5576(85)	0.3327(42)
28	48×60	0.5462(53)	0.6725(148)	0.4071(57)
32	40×48	0.6297(58)	0.7760(151)	0.4607(66)
36	40×48	0.7031(70)	0.8658(201)	0.5277(61)
40	48×48	0.8003(68)	0.9625(243)	0.5955(89)
44	48×48	0.8950(112)	1.0866(329)	0.6561(119)
48	48×48	0.9674(163)	1.1767(326)	0.7291(139)
52	52×52	1.0658(250)	–	0.7845(207)
64	64×64	–	–	0.954(38)

Table 4: The energies, $E(l)$, of the lightest flux tubes of length l (all l in lattice units) and $p = 0$, and with the flux belonging to the indicated representations. For SU(6) at $\beta = 171.0$.

statistical uncertainty of about $\pm 1\%$. For the higher representations there are still visible corrections for $l_{\perp}/a = 40$ but $l_{\perp}/a \geq 60$ appears to be safe at the ± 2 or 3 percent level of our statistical errors. It thus appears that $l_{\perp}/a = 100$ is in fact a very safe and conservative choice. This provides further evidence that the energies calculated in this paper are not afflicted by significant finite size corrections.

In Table 6 we again show some results for the ground states (and also for some excited states) in various representations, but this time for a much longer flux tube, $l/a = 40$. This confirms that a transverse size $l_{\perp}/a = 32$ is already large enough, and the sizes we have actually used are very conservative.

Finite size corrections also affect the screening of one representation to another, as shown in Tables 2,3 of [7]. This is relevant because it is only when the screening is very weak that we can categorise the states as being (almost entirely) in $k = 2A$ and $k = 2S$ rather than just $k = 2$ (and similarly for our other representations). We therefore perform a similar analysis here. We define the normalised overlap

$$O_{2AS}(b) = \frac{\langle \Phi_{2A,b}^{\dagger}(t=0) \Phi_{2S,b}(t=0) \rangle}{\langle \Phi_{2A,b}^{\dagger}(t=0) \Phi_{2A,b}(t=0) \rangle^{1/2} \langle \Phi_{2S,b}^{\dagger}(t=0) \Phi_{2S,b}(t=0) \rangle^{1/2}} \quad (11)$$

where $\Phi_R(t)$ is the simple Polyakov loop at blocking level b and representation R , in the time-slice $t = 0$ and, as usual, summed over spatial sites so as to have zero transverse momentum. (Obviously we will average over all equal times.) The range of values of b is restricted by the fact that a ‘blocked link’ [22, 6] joins lattice sites that are separated by 2^{b-1} lattice sites. So for $l/a = 16$ it only makes sense to consider $1 \leq b \leq 5$. Essentially, loops at blocking level b are smeared over distances significantly greater than this separation 2^{b-1} . Thus the highest blocking level shown typically involves operators that overlap over the boundary of the torus

$aE_R(l = 16; l_\perp)$					
R	$l_\perp = 20$	$l_\perp = 40$	$l_\perp = 60$	$l_\perp = 80$	$l_\perp = 100$
f (k=1)	0.0742(10)	0.0781(8)	0.0781(11)	0.0766(13)	0.0777(3)
k=2A	0.1167(18)	0.1385(18)	0.1430(28)	0.1460(20)	0.1460(14)
k=2S	0.2335(18)	0.2243(19)	0.2260(31)	0.2280(24)	0.2256(29)
k=3A	0.1292(32)	0.1624(26)	0.1706(35)	0.1748(26)	0.1742(11)
k=3M	0.2521(48)	0.2573(40)	0.2675(64)	0.2699(60)	0.2705(61)
k=3S	0.4148(41)	0.364(12)	0.390(9)	0.421(5)	0.409(4)
Adj (k=0)	0.1553(44)	0.1652(30)	0.1692(47)	0.1796(44)	0.1658(66)

Table 5: The energy, $E_R(l)$, of the lightest flux tube of length $l = 16$ (all l in lattice units) on a $16 \times l_\perp \times 200$ lattices, and with the flux belonging to the representation R . For SU(6) at $\beta = 171.0$.

and these can be affected by strong finite volume corrections.

Bearing the above in mind, we show our results for the overlap $O_{2AS}(b)$ in Table 7. We remark that the calculations with $l/a \neq 16$ are mostly with lower statistics, designed to be sufficient for our purposes here. We also calculate Polyakov loops in the (usually) longer y direction, and this gives us some values of $O_{2AS}(b)$ at small l_\perp (now $= l_x$) and larger l (now $= l_y$) which we also present in Table 7. We conclude from this Table that:

- 1) for very small l the overlap $|O_{2AS}(b)|$ is large for all b ;
- 2) and for fixed l the values of $|O_{2AS}(b)|$ grow as l_\perp decreases;
- 3) but $|O_{2AS}(b)|$ rapidly decreases to values consistent with zero as $l \rightarrow \infty$, and this is so for any fixed b and appears to be the case for any fixed l_\perp as well.

We conclude that for long flux tubes on large volumes, we can safely ignore screening and label states as $k = 2A$ and $k = 2S$. Indeed we see that it is only when l or l_\perp are close to the phase transition at l_c that screening is significant. Our results for $k = 3A, 3M, 3S$ are very similar and the vacuum expectation value of the adjoint loop shows very similar trends. In practice this means that in Tables 3, 4 it is only for $l/a = 16$ (and $l/a = 20$ for some $k = 3$) that the states have needed to be extracted using the whole $k = 2$ or $k = 3$ basis (and we have then assigned the A, M, S labels on the basis of what component dominates the wave function).

4.2 k=2A, 2S

In the $k = 2$ sector we focus on the irreducible representations in $f \otimes f$, i.e. the totally antisymmetric, $2A$ and the totally symmetric, $2S$ [16]. The $k = 2$ sector contains other representations, e.g. from the decomposition of $f \otimes f \otimes f \otimes \bar{f}$, but one expects these to have higher energies, and we do not consider them here. As we have remarked above, the dynamics appears to respect these representations very well, despite the potential mixing from gluons in the vacuum. Only for $l \sim l_c$ is there significant mixing.

The lightest $k = 2$ flux tube is essentially pure $k = 2A$. We see from Table 3 that it

$aE_R(l = 40; l_\perp)$			
R	$l_\perp = 16$	$l_\perp = 32$	$l_\perp = 48$
f (k=1)	0.2790(24)	0.2802(28)	0.2817(14)
f (k=1)★	0.527(10)	0.522(7)	0.507(3)
k=2A	0.438(4)	0.465(7)	0.462(5)
k=2A★	0.718(4)	0.663(11)	0.655(11)
k=2S	0.673(5)	0.661(7)	0.650(9)
k=3A	0.484(9)	0.530(8)	0.526(7)
k=3A★	0.774(18)	0.719((10)	0.732(15)
k=3M	0.814(7)	0.799(24)	0.817(13)
k=3S	1.14(2)	1.116(16)	1.154(29)
Adj (k=0)	0.566(6)	0.584(10)	0.560(9)

Table 6: The energy, $E_R(l)$, of the lightest flux tube of length $l = 40$ (all l in lattice units) on a $40 \times l_\perp$ spatial volume, and with the flux belonging to the representation R . For SU(6) at $\beta = 171.0$.

is lighter than two fundamental flux tubes (which would also be $k = 2$) so this flux tube is absolutely stable. Its calculation therefore provides a ‘benchmark’ for what constitutes a ‘good’ energy calculation in this paper. The energy is calculated from the correlator $C(t = an_t)$ of our variationally selected best trial wave-functional for the state. We can define an effective energy by

$$aE_{eff}(n_t) = -\ln \frac{C(n_t)}{C(n_t - 1)} \quad (12)$$

and note that if $C(t)$ is independent of t for $t \geq t_0$ (within errors), then this implies that it is given by a single exponential, $C(n_t)/C(0) = |c|^2 e^{-aEn_t}$ for $t \geq t_0$ (within errors). So to calculate aE we need to identify a plateau in the values of $aE_{eff}(n_t)$ and the quality of our calculation is reflected in how convincing this plateau is.

In Fig. 1 we plot our values of $aE_{eff}(n_t)$ for various values of l . We also show our final energy estimate in each case by the horizontal lines. We have excluded values at larger n_t , once the errors have become larger than $\sim 15 - 20\%$ since these carry little information and merely clutter the plot. (In addition, at large n_t the correlations within the Monte Carlo sequence become very long and our error estimates become increasingly unreliable.) We can see that we have a well-defined energy plateau for all our values of l , although the length of the plateau shortens as $l \uparrow$ since $e^{-E_n t}$ will disappear into the statistical noise more quickly with increasing t for larger E_n .

We fit these energies with the Nambu-Goto formula in eqn(10), together with a theoretically motivated $O(1/l^7)$ correction, which however plays no significant role in the fit. We extract the string tension $a^2\sigma_{2A}$ and plot in Fig 2 the values of $E_0(l)$ versus l , with both expressed in units of the string tension. We see a very clear near-linear increase characteristic of linear confinement. We also see that the pure Nambu-Goto prediction appears to fit very

2A/2S overlap							
l	$l_\perp \times l_t$	bl=1	bl=2	bl=3	bl=4	bl=5	bl=6
13	60×200	0.292(48)	0.344(53)	0.384(56)	0.438(58)	–	–
14	60×200	0.122(25)	0.157(31)	0.187(36)	0.227(42)	–	–
16	20×200	0.172(6)	0.234(7)	0.285(8)	0.356(9)	0.491(8)	–
16	40×200	0.053(3)	0.076(4)	0.097(5)	0.129(6)	0.206(8)	–
16	60×200	0.036(3)	0.053(4)	0.067(5)	0.088(6)	0.136(8)	–
16	80×200	0.034(2)	0.048(3)	0.061(4)	0.081(5)	0.122(6)	–
16	100×200	0.032(3)	0.047(3)	0.059(4)	0.076(5)	0.116(7)	–
20	16×200	0.071(2)	0.125(3)	0.175(3)	0.259(4)	0.416(3)	–
40	16×200	0.001(1)	0.002(1)	0.009(1)	0.035(2)	0.189(2)	–
60	16×200	0.000(1)	0.001(1)	0.000(1)	0.006(1)	0.090(2)	–
80	16×200	0.001(1)	0.001(1)	0.001(1)	0.001(1)	0.041(2)	–
100	16×200	0.000(1)	0.001(1)	0.001(1)	0.000(1)	0.020(1)	–
20	70×120	0.010(5)	0.015(8)	0.019(12)	0.028(16)	0.037(19)	–
24	48×60	0.002(4)	0.001(5)	0.003(7)	0.011(9)	0.022(13)	–
32	40×48	0.001(4)	0.003(3)	0.000(6)	0.003(7)	0.001(11)	0.107(17)
48	48×48	0.001(3)	0.001(3)	0.003(5)	0.001(6)	0.004(5)	0.011(5)

Table 7: The modulus of the normalised overlaps $|O_{2AS}(bl)|$ of blocked Polyakov loops in the 2A and 2S representations, for blocking levels bl, as defined in eqn(11). On lattices of various sizes (shown in lattice units).

well.

Uniquely for the absolute ground state the expansion of the Nambu-Goto prediction for the energy $E_0(l)$ in powers of $1/l^2\sigma$ converges right through the range of l where we have calculations; indeed all the way down to $l\sqrt{\sigma} = \pi/3 \sim 1.1 < l_c\sqrt{\sigma}$. This provides an opportunity to test not just the resummed Nambu-Goto expression, but the individual power correction terms predicted to be universal [3]. To do this we normalise $E_0(l)$ to the leading σl piece, so that we can readily expand the scale, and compare to various ‘models’ for $E_0(l)$. This produces Fig. 3. Here we see that the free string expression is good all the way down to $l\sqrt{\sigma_{2A}} \sim 2$ which is close to the deconfining length, l_c , indicated by the vertical red line. And we note that a $O(1/l^7)$ correction can describe the deviations from Nambu-Goto for $l\sqrt{\sigma_{2A}} \leq 2$. However we also see that including just the leading universal correction, i.e. $E_0(l) = \sigma l - \pi/6l$ [1, 2], is indistinguishable from Nambu-Goto within the errors in the range of l where the latter well describes $E_0(l)$. However if we only include a linear σl piece, then this does not fit at all. Thus we have a quite accurate confirmation of the presence of the universal Lüscher correction, but not really much more than that. The reason for this is that the universal corrections to $E_0(l)$ have small coefficients, since they represent just the zero-point energies of the string fluctuation modes, which indeed is why the expansion converges down to small l . (One can do better with the fundamental flux tube [6], since σ is smaller there, and it is in

that case that one may realistically hope to pin down all the universal corrections.)

It is worth quantifying how well we can constrain the Lüscher correction with the $k=2A$ ground state. We find

$$aE_{2A}(l) = \sigma_{2A}l - c_{eff}\frac{\pi}{6l} \quad ; \quad c_{eff} = 1.05(15) \text{ for } l\sqrt{\sigma_{2A}} \geq 2.5, \quad (13)$$

which is a usefully accurate test of this universal coefficient.

We now turn to states with non-zero longitudinal momenta. In Fig. 2 we also plot the ground state energies for the lowest two non-zero momenta along the l -torus, $p = 2\pi/l$ and $p = 4\pi/l$. We find that there is a unique such state for $p = 2\pi/l$ and it has $P = -$. For $p = 4\pi/l$ we find two apparently degenerate ground states, one with $P = +$ and one with $P = -$. All this is just as expected from Nambu Goto where the $p = 2\pi/l$ state has one phonon, and hence $P = -$, and the $p = 4\pi/l$ ground states have either one phonon carrying the whole momentum, with $P = -$, or two phonons sharing the momentum, and hence $P = +$. We also show in Fig. 2 the ground state energy of two (non-interacting) fundamental flux tubes of length l carrying the same total momentum. We see that this state always has a higher energy than that of the corresponding $k = 2A$ flux tube showing that the latter is indeed stable.

Since the only parameter in Nambu-Goto is the string tension, which is obtained by fitting the $p = 0$ state, the Nambu-Goto predictions shown for $p = 2\pi/l$ and $p = 4\pi/l$ have no free parameters. It is therefore remarkable that the agreement is so precise and extends to our smallest values of l . Of course some of the energy comes from p^2 and so it is useful to perform a comparison with this subtracted. We therefore define the quantity:

$$\Delta E^2(q, l) = E^2(q; l) - E_0^{NG\ 2}(l) - \left(\frac{2\pi q}{l}\right)^2 \stackrel{NG}{=} 4\pi\sigma(N_L + N_R), \quad (14)$$

using eqns(3) and (10). This exposes the excitation energy predicted by Nambu-Goto. We plot the ratio $\Delta E^2(q, l)/4\pi\sigma$ in Fig. 4. We see that the integer-valued contribution of the excitation energy is very accurately confirmed for all l , even for very short flux tubes which certainly do not ‘look like’ thin strings. This is something that we have already observed for fundamental flux tubes [6] but here we know that the flux tube is a bound state with, therefore, some extra internal structure. From the comparison in Fig. 2 between the $k = 2A$ energy and that of two free $k = 1$ flux tubes, we infer that the binding energy is not very large, so that at small l the $k = 2A$ flux tube will be a ‘blob’ rather than a ‘thin string’. It is therefore remarkable that its excitation spectrum should be so precisely that of a free thin string.

In Fig. 4 we also show what happens if one excludes the zero-point energy from the Nambu-Goto formula. We see a very visible shift for both $p = 0$ and $p = 2\pi/l$. (It would be pointless to go to higher p since the errors are too large there.) For $p = 0$ this is just another presentation of our result in eqn(13), however it is interesting to see that the $p \neq 0$ spectrum also reveals the presence of this zero-point energy. We do not quantify it further because it would add little to eqn(13).

To assess the significance of these results for $p \neq 0$ it is worth stepping back and asking what we might expect if we make no assumption at all about the relevance of stringy fluctuations. We would expect on general grounds that the absolute ground state of the flux tube is intrinsically translation invariant in the direction of the flux tube, so can only have $p = 0$. Thus the non-zero p has to be carried by some additional excitation. Let us suppose that this is some particle of mass m . Then neglecting any interaction between this particle and the flux tube, the energy of the combined system is

$$E(l; p) = E_{gs}(l) + (m^2 + p^2)^{1/2} \quad ; \quad p = \frac{2\pi q}{l} \quad (15)$$

where $E_{gs}(l)$ is the (observed) energy of the absolute ground state. To decide whether this model has any plausibility, we plot $E(l; p)$ for the massless case, $m = 0$, in Fig. 2 as the dashed lines. We see that these are very close to the Nambu-goto predictions and could provide a good first approximation to the observed spectrum. It is therefore interesting to ask how this constrains the value of m . So we calculate m using eqn(15) at each value of l for $p = 2\pi/l$, since these $p \neq 0$ energies are the most accurate, and average the results for $l \geq l_0$, for various choices of l_0 . The result, in units of the string tension, is shown in Fig. 5. (We also show the similar result of a similar analysis applied to flux tubes in the $k = 3A$ representation.) Roughly speaking this tells us that $m^2/\sigma_{2a} \lesssim 0.1(1)$. This is to be compared to the known value of the mass gap in the SU(6) gauge theory [23, 24] which is $m_G^2/\sigma_{2a} \sim 13$. Thus this ‘particle’ cannot be an excitation in the bulk space-time, and must be an excitation that lives on the flux tube. In that case the obvious candidate is a massless stringy mode of the kind described by the Nambu-Goto free string model. Note that this of course means that the relationship in eqn(15) is not the correct one. Note also that although eqn(15) is, numerically, very close to eqn(3) for states where the massless phonons are either all right or all left movers, this is no longer the case when both right and left movers are present, e.g. the first excited $p = 0$ state. As it happens, we shall shortly see that, although this state is badly described by the extension of eqn(15), it is also badly described by Nambu-Goto. However in the case of fundamental flux tubes, studied in [6], one finds that Nambu-Goto works well for l not very small, and thus eqn(15) would be strongly disfavoured. In addition a state with a ground state $p = 0$ flux tube and an additional particle would not couple to our operators as $N \rightarrow \infty$ in contrast to what one observes for the states with $p \neq 0$. Our purpose in considering this simple model was to establish, in a pedestrian way, that one must look to massless modes living on the flux tube for the origin of the observed spectrum.

We turn now to the spectrum of excited states with $p = 0$. We plot, in Fig 6, the four lightest $P = +$ states, and the two lightest $P = -$ ones, as well the predictions of Nambu-Goto for the lowest few energy levels. (We also plot some higher excitations for $l = 32a$ and $l = 52a$, which we shall return to shortly.) In Nambu-Goto the ground state, with no phonons, is non-degenerate, with $P = +$, as is the first excited energy level which has one left and one right moving phonon with momenta $p = \pm 2\pi/l$. The next energy level has four degenerate states with the left and right moving phonons sharing twice the minimum momentum. Since this can be carried by one or two phonons, two of these states have $P = +$ and two have $P = -$. If the $2A$ flux tube states were close to Nambu-Goto, as they turn out to be for

the case of fundamental flux, we should find our calculated energies clustering closely about the lowest three Nambu-Goto energy levels. While we do indeed observe in Fig 6 that the lightest two states do have parity $P = +$, and the next two $P = +$ states are roughly in the same energy range as the lightest two $P = -$ states, we see nothing like the (near)degeneracy predicted by Nambu-Goto. There is some evidence that the first excited $P = +$ state and the lightest $P = -$ state approach the appropriate Nambu-Goto levels, and that the second lightest $P = -$ state agrees with the Nambu-Goto prediction for all but the smallest values of l . However the observed excited states are, in general, far from showing the Nambu-Goto degeneracies and are far from the Nambu-Goto predicted energies, even for the largest values of $l\sqrt{\sigma}$. While the first excited state appears to clearly approach the string prediction, even here it would be useful to have some further evidence that it is asymptoting to that curve and not just crossing it. It is useful to recall that for the fundamental flux tube [6], the convergence to Nambu-Goto was rapid and unambiguous (albeit not as rapid as for the ground state). The messiness of the picture in Fig 6 is of course what one would have naively expected for such a bound state flux tube, and the real surprise is the precise stringy behaviour we have observed for the lightest states with non-zero momenta. One significant difference with the latter is that here the states are generally well above the threshold for decay. The lightest asymptotic decay products will be two fundamental flux tubes with equal and opposite transverse momentum. The energy of the threshold, corresponding to zero relative momentum, is shown in Fig 6 and one is tempted to note that the deviation of the first excited state from Nambu-Goto decreases as the phase space for decay decreases. We also show the energy of a decay state composed of a glueball and a ground state $k = 2A$ flux tube. We see that this is quite high and, in addition, such a decay will be large- N suppressed.

To provide some more context for these states, we have also shown in Fig 6 the next 6 $P = +$ and 5 $P = -$ states for $l = 32a$ and $l = 52a$ (slightly shifted in l for clarity). The number of states is motivated by the fact that the next Nambu-Goto energy level has 5 $P = +$ and 4 $P = -$ degenerate states, so we are also including at least one state, for each P , that will approach a yet higher energy level as $l \rightarrow \infty$. (But note that the extraction of the energies can be ambiguous for these massive states.) The main message, considering all the $l = 32a, 52a$ states, is that there is no visible clustering in the energy of the states that might suggest that they are converging to the Nambu-Goto energy levels, except for the absolute ground state and perhaps the first excited state, both of which are $P = +$ at our largest value of l where a clear gap has opened between them and the $P = -$ states – as expected in Nambu-Goto. For the first excited state there is a residual ambiguity: is it the first excited state at lower l that asymptotes to the Nambu-Goto level as $l \rightarrow \infty$, or is it perhaps the second, with the first ‘crossing’ that level somewhere between $l = 52a$ and $l = 64a$? In fact our analysis in Section 5 will address and resolve this issue. What we see in Fig 6, particularly for $l = 52a$, is very much a continuous distribution of excited states without any obvious level structure. This makes it hard, for example, to know whether the near-coincidence of the second $P = -$ energy with the Nambu-Goto prediction is in fact significant, or merely the chance result of this near-continuous distribution of states. What is clear from Fig 6 is that we are very far from the values of l where the Nambu-Goto spectrum might become a good first approximation for these states.

The fact that these excited $p = 0$ states are generally well above their decay thresholds raises some questions. The most important is how confident can we be that we have extracted their ‘energies’? If the decay width is very small, the propagator should have a pole in the complex energy plane very close to the real axis, and we would expect correlators designed for stable states to behave just as they do for a stable state, within the finite statistical errors, i.e. we should see an effective energy plateau that is lost in the statistical errors at larger t before deviations from the plateau become visible. We show the effective energy plateaux for the first excited state in Fig. 7. We see that for large l these plateaux are unambiguous and not so different from those of our stable ground state in Fig. 1. As l decreases, however, the apparent plateau shifts to larger t and becomes increasingly ambiguous. This is very different to what we observe in Fig. 1. The likely reason for this is that the phase space for the decay of the first excited state grows as l decreases (as we can infer from Fig 6), and so presumably does the decay rate. So it is interesting to perform a different analysis, at the smallest values of l , that attempts to take this finite decay width into account. The relevant asymptotic states in this energy range are those composed of two (unexcited) fundamental flux tubes with equal and opposite transverse momenta. (Flux tubes with longitudinal momenta have larger energies.) Obviously if we performed a variational calculation with a complete basis of $k = 2$ operators, then these are the states we would obtain. However the operators we actually use are all of the form $\text{Tr}_{2A}\{l_p\} \propto \text{Tr}_f\{l_p\}^2 - \text{Tr}_f\{l_p^2\}$ with l_p some winding operator. The $\text{Tr}_f\{l_p\}^2$ piece represents two fundamental flux tubes at zero spatial separation, which can be re-expressed as a sum over all relative momenta. However the projection onto any such state with given momentum will be very small, so a variational calculation performed at $t = a$, as ours is, will not pick out these states. However the overall projection onto all these states is not small, and a heuristic procedure is to perform a fit to the correlation function that is in terms of these asymptotic scattering states, but with an amplitude that encodes a slightly unstable state. We choose, again heuristically, a Breit-Wigner form. So we fit to:

$$C(t) = \sum_{\vec{p} \neq 0} |c_{BW}|^2 e^{-E(p)t} \quad ; \quad E(p) = 2E_f(p), \quad |c_{BW}|^2 = \frac{c}{(E - E_0)^2 + (E_0\Gamma_0)^2} \quad (16)$$

where E_f is the lightest energy of a fundamental flux tube with transverse momentum p , c is a constant fixed by normalisation, E_0 is the real part of the pole energy and Γ_0 the (full) width. We either sum over a discretisation of the momentum integral, or use the transverse momenta dictated by the size of the transverse torus. (In practice it does not matter which we use.) In Fig 8 we display the values of aE_{eff} for $l = 16a$, on a blown-up scale, and display different fits. The red line arises from a conventional fit with an excited state in addition to the desired lightest state. Here the lightest state is at $aE = 0.25$, and the heavier one is at $aE = 0.49$, with relative probabilities 15% and 85% respectively. With such a low overlap, we can have little confidence in the robustness of this lightest state. The alternative fit based on eqn(16) is shown by the solid black line and corresponds to $aE_0 = 0.475$ and $\Gamma_0 = 0.065$. (The dotted black line corresponds to a sum over scattering states with uniform probability.) We see that the value of the energy is close to but larger than $E_{eff}(t = a)$ whereas a search for a large- t plateau leads (as in our first fit above) to a much lower result. This is characteristic of such fits. We note that it is no coincidence that in our first, conventional, fit the dominating ‘excited’ state

at $aE = 0.49$ is close to our Breit-Wigner pole in the alternative fit based on eqn(16). This gives us confidence that this is most likely the actual energy of this unstable excited state. We note that applying such a procedure would raise the energy estimate significantly closer to the Nambu-Goto prediction. For example, a similar analysis at $l = 20a$ would give $aE_p = 0.485$, with $\Gamma_p = 0.050$, rather than the value $aE \simeq 0.38$ from a plateau estimate, and this would approximately halve the discrepancy with Nambu-Goto. The effect is even more marked at $l = 16a$. Clearly what we need is sufficient statistical accuracy to distinguish between the two different $n_t \rightarrow \infty$ values of $aE_{eff}(n_t)$ in Fig 8. Moreover it would be useful to see the stability of such an analysis to the presence of a second heavier excited state (which surely contributes at some level). Nonetheless, while we cannot be definitive on this, it is plausible that where the apparent plateau is indistinct because it is at large n_t , and in addition the state has a large phase space to decay, the actual energy of the ‘resonant’ flux tube is much closer to the value of $aE_{eff}(t \rightarrow 0)$ than to $aE_{eff}(t \rightarrow \infty)$. In the present case this would suggest values for the first excited state that are closer to the Nambu-Goto prediction at small l than our conventional estimates shown in Fig 6. So it is not possible for us to be certain how much of the large apparent deviation from Nambu-Goto is due to the extra modes associated with the internal structure of the $k = 2A$ flux tube, and how much is a consequence of the fact that these states are unstable.

Two remarks. The first is that none of the above caveats apply to the ground states with $p \neq 0$ shown in Fig. 2. Here the effective energy plateaux (which we do not show) start at small t and typically become increasingly well-defined as l decreases. The second remark is that one might wonder if some of the apparent downward drift in $E_{eff}(n_t)$ that we see at large n_t in Fig. 7 is not due some small admixture of the ground state in our variationally estimated excited state wave function. Since our variational ground state wave function has a typical overlap onto the ground state of $\sim 0.985(15)$ (which can be inferred from the $E_{eff}(n_t)$ values shown in Fig. 1) we can estimate the maximum such contribution to the excited $E_{eff}(n_t)$ in Fig. 7, and it turns out to be invisible for $l/a \geq 24$ (at our level of accuracy) and only possibly becomes visible for $n_t \geq 15$ for $l/a = 16, 20$. That is to say, it is essentially irrelevant here.

We turn now to flux tube states obtained by performing calculations with operators projected onto the $k = 2S$ representation, i.e $\text{Tr}_{2S}\{l_p\} \propto \text{Tr}_f\{l_p\}^2 + \text{Tr}_f\{l_p^2\}$ with l_p some winding operator. (For the $l = 16a$ $p = 0$ ground state we obtain a cleaner variational state by using the full $2A \oplus 2S$ basis, and that is what we show here. The admixture of $2A$ is small and so it still makes sense to label the state as $2S$, as we do.) We know that these will be heavier than the corresponding $k = 2A$ states [16, 8] and so we expect all of them to be unstable as well as having larger statistical errors. In Fig. 9 we show the ground states with the lowest longitudinal momenta. We also show the energies of the lightest decay products in each case. Just as for $k = 2A$ the energies are remarkably close to the Nambu-Goto predictions, as emphasised by comparing the actual excitation energies in Fig. 10. In Fig. 11 we show the effective energies for the absolute $p = 0$ ground state. We also indicate the expected decay thresholds on the right side of the figure. It seems clear that $E_{eff}(n_t)$ does possess extended plateaux very different from the decay thresholds in the lowest l cases where we have accurate results to large t . So while the quality of the calculations is markedly inferior to the $k = 2A$ case, we have confidence in our extraction of the energies plotted in Fig. 9. The

situation with the excited $p = 0$ states is however much worse and we are unable to extract the corresponding energies. Our problem is illustrated by Fig. 12 where we plot the effective energies for the ‘state’ selected by our variational procedure as the first excited $p = 0$ state. We cannot identify a plausible energy plateau for any value of l , and $E_{eff}(n_t)$ is consistent with a decrease towards the decay thresholds shown. In Fig. 13 we repeat the exercise in Fig 8, now for the $l/a = 16$ $k = 2S$ flux tube. The fit using eqn(16) works very well, and corresponds to an energy $E_0 = 0.58$ and a width $\Gamma_0 = 0.1$. The two exponential fit is less convincing and corresponds to energies 0.205 and 0.595 with overlaps squared of 0.1 and 0.9 respectively. This begins to point rather unambiguously to an energy estimate of $E \sim 0.58$ and hence $E/\sqrt{\sigma_{2S}} \sim 4.6$ at $l\sqrt{\sigma_{2S}} \sim 2.1$. We note that this is below, but not far below, the Nambu-Goto prediction. A similar conclusion follows for $l/a = 20$. It is thus plausible that this unstable first excited state is indeed quite close to Nambu-Goto although this would be far from apparent using a conventional analysis.

4.3 $k=3A, 3M, 3S$

In the $k = 3$ sector we focus on the irreducible representations in $f \otimes f \otimes f$, which are the totally antisymmetric, $3A$, the mixed, $3M$, and the totally symmetric, $3S$. We know from earlier work [16, 8] that the corresponding string tensions are very close to the predictions of Casimir scaling (see also Table 2) and so, as we shall see, the ground $3A$ states are stable, the $3M$ states nearly so, and the $3S$ states are highly unstable.

In Fig. 14 we plot the lightest energies of $k = 3A$ flux tubes with longitudinal momenta $p = 0, 2\pi/l, 4\pi/l$. Just as for the corresponding $k = 2$ flux tubes, we see excellent agreement with Nambu-Goto all the way down to $l \sim l_c$. The relevant asymptotic decay states are not just 3 fundamental flux tubes, but also a stable $k = 2A$ flux tube with a fundamental one. The latter is lighter and the thresholds for both are plotted as the black lines in Fig. 14, demonstrating the stability of the $k = 3A$ states. As we see in Fig. 15, for the absolute ground state, we have very well defined energy plateaux, again just as for the $k = 2A$ flux tubes.

As for the $k = 2A$ case, it is worth quantifying how well we can constrain the Lüscher correction with the $k = 3A$ ground state. Here we find

$$aE_{3A}(l) = \sigma_{3A}l - c_{eff}\frac{\pi}{6l} \quad ; \quad c_{eff} = 1.11(11) \text{ for } l\sqrt{\sigma_{3A}} \geq 2.3, \quad (17)$$

which is again a usefully accurate test of this universal coefficient.

We turn now to the lightest excited states in the $p = 0$ sector, as displayed in Fig. 16. Comparing to Fig. 6 we see that the phase space for the first excited flux tube to decay is smaller here and indeed at larger l it is stable. This is perhaps why its energy, particularly at small l , is closer to Nambu-Goto than in the $k = 2A$ case. And also why the effective energies displayed in Fig. 17 show clear plateaux even for $l/a = 16$, in contrast to the $k = 2A$ case in Fig. 7. (Note that for $l/a = 16$ we use our full $k = 3$ basis, which means that state includes a very slight admixture of $k = 3M$ and $k = 3S$.) The decay thresholds are indicated on the right hand axis of Fig. 17, and it is clear that the low- l plateaux take very different values. This provides us with a quite clean example of an excitation of a bound state flux tube where

we can ignore the (slight) instability of the state. It is therefore interesting to compare this to the corresponding excitation of the fundamental flux tube in Fig.19 of [6]. We see that the deviation from Nambu-Goto is indeed very much larger here, and this must be due to the bound state structure of this flux tube. We note that a similar analysis applied to the first $P = -$ excitation with $P = 2\pi/l$ leads to very similar conclusions.

We turn now to the heavier $k = 3M$ states. We plot in Fig. 18 the ground states with the lowest longitudinal momenta. Once again these particular states agree very well with the Nambu-Goto predictions. However we see that they are now slightly above the decay threshold and so will be unstable but apparently not enough to affect the extraction of, for example, the absolute ground state as we see in Fig. 19. (Again we use the full $k = 3$ basis for the $l/a = 16$ ground state.) However the $p = 0$ excited states are very unstable and we are unable to identify useful plateaux.

The $k = 3S$ states are much heavier and we can only estimate energies for the ground state $p = 0, 2\pi/l$ states, as shown in Fig. 20. Again we see rough agreement with Nambu-Goto, but now the decay phase space is large – becoming very large for large l . We show the effective energies for the absolute ground state in Fig. 21. While the plateaux at lower l are quite clear and are far from the decay thresholds (indicated on the right hand axis), this is not the case at the largest values of l . (Indeed we do not even attempt to extract an energy for $l/a = 48$.) In the latter cases, while the motivation for our energy estimates should be apparent, it is not necessarily convincing. Nonetheless the usual agreement with Nambu-Goto for such states at smaller l is remarkable.

4.4 adjoint

The adjoint flux tube appears in $f \otimes \bar{f}$ and should couple to operators $\text{Tr}_{adj} l_p = |\text{Tr}_f l_p|^2 - 1$, if indeed it exists. There is some evidence from the calculation of adjoint potentials that it does indeed exist and that the adjoint string tension satisfies approximate Casimir scaling (see e.g. [19] and references therein). Such a flux tube can be screened down to the vacuum by gluons, but this is suppressed by $1/N^2$, and is in fact negligible except for finite volume effects. The latter can either arise if l is small, i.e. $l \sim l_c$, or if we consider blocked/smear l_p operators that extend around the transverse torus. In practice we always include such highly smeared operators in our calculations, since they (slightly) improve the overlap onto the ground state of the adjoint flux tube, and we therefore explicitly subtract vacuum expectation values in our correlators.

An adjoint flux tube whose string tension satisfies approximate Casimir scaling will in general be heavier than a pair of fundamental anti-fundamental flux tubes and can therefore decay into these. (Here there is no large- N suppression.) Just as with unstable k -strings, the important question is whether the adjoint flux tube is nearly stable, so that conventional methods for extracting the energy can be used, or not. We shall be careful to establish whether this is so or not.

In Fig. 22 we plot the energies of the lightest adjoint flux tubes with longitudinal momenta $p = 0, 2\pi/l, 4\pi/l$. As usual the $p = 0$ Nambu-Goto fit fixes the string tension $a^2\sigma_{adj}$, and then the Nambu-Goto predictions for $p \neq 0$ are parameter-free. We observe that, again as usual,

these predictions are remarkably well satisfied all the way down to $l \sim l_c$. The decay thresholds are indicated and we see that the decay phase space is small, raising the hope that the decay widths will be negligibly small. Of course the statistical errors are quite large here so it is worth extracting the ‘excitation energy’ as defined in eqn(14) to see how well that is being determined. As we see from Fig. 23 the modes carrying momentum are indeed unambiguously the wave-like modes of a thin relativistic string.

In Fig. 24 we plot the effective energies for the absolute ground state. (Energies shifted for clarity.) Horizontal red solid lines indicate our plateau estimates, including errors. For small and medium l these are well determined, but for the largest values of l the states are very massive and we quickly lose the signal as we go to larger n_t . Hence the generous error estimates in these cases. For comparison we plot the $f\bar{f}$ threshold energies as horizontal dashed lines (also as points on the right hand axis). These are quite close to the plateaux, especially at small l . So we blow up the scale for the latter states in Fig. 25. A characteristic feature of effective energies is that once the error gets large, the estimate of that error becomes unreliable. This applies to the large n_t decrease or increase in $aE_{eff}(n_t)$ that we see in Fig. 25. Since our correlators are diagonal, an increase would violate positivity, and so must be statistical. There is therefore no reason to take the decreases any more seriously. Given these remarks, we can see that the $l/a = 16$ plateau estimate is consistent with the decay threshold, while for $l/a \geq 20$ (and unambiguously for $l/a > 20$) the plateaux is well above the threshold. We conclude that the adjoint flux tube does indeed exist as a distinct and nearly stable ‘bound state’.

On the other hand we cannot identify well-defined excited states with $p = 0$. These would have a very large phase space for decay into $f\bar{f}$ flux tubes, so this is not unexpected. They are presumably analogous to broad resonances, and will be equally difficult to identify.

4.5 84 and 120

In the $f \otimes f \otimes \bar{f}$ sector of $SU(6)$, the irreducible representations with the smallest Casimirs and, we can assume, the smallest string tensions, are the 84 and 120. (See the Appendix.) Here we shall study flux tubes carrying flux in these two representations.

Such flux tubes can mix with single fundamental flux tubes, but this is large- N suppressed and given our experience with the adjoint flux tube, we shall (usually) ignore this possibility. However the decay/mixing with 3 (anti)fundamental flux tubes is not large- N suppressed. And neither is that with a $k = 2A$ and an antifundamental, which is even lighter. In Fig. 26 we plot the energies of the ground state 84 flux tubes with longitudinal momenta $p = 0, 2\pi/l, 4\pi/l$. The Nambu-Goto predictions are shown as solid red curves, with the decay $3f$ and $2A + f$ thresholds indicated by the black curves. As usual we extract the string tension from the $p = 0$ fit so that the $p \neq 0$ predictions are parameter free. We observe that the agreement is, once again, remarkably good for $p = 2\pi/l$ and quite good for $p = 4\pi/l$, where however the states are very massive and it becomes difficult to identify plausible plateaux. The string tension is comparable to that for $k = 3M$ (see Table 2) as is the phase space for decays. So it is no surprise that, just as for $3M$, we are unable to obtain energy estimates for $p = 0$ excited states. The ground state however has reasonably clear energy plateaux, as we see in Fig. 27,

at least for $20 \leq l/a \leq 40$. For $l/a \geq 44$ the effective energies are large and disappear rapidly into the statistical noise as n_t increases, making plateau identification increasingly subjective. For $l/a = 16$ we see no plateau, and here we see that $E_{eff}(n_t)$ decreases well below the decay thresholds shown and appears to be asymptoting to a large- N suppressed single f admixture. That this should only occur for our shortest flux tube, $l/a = 16$, is consistent with our earlier observations about the finite volume effects displayed in Table 7.

In Fig. 28 we plot the ground state energies of flux tubes in the 120 representation for $p = 0, 2\pi/l$. The 120 string tension, which we obtain by fitting the $p = 0$ values, is almost as large as the $k = 3S$ one, and so it is no surprise that just as in that case we have no useful results for $p = 4\pi/l$ or for any excited states. Indeed even the $p = 0$ effective energy plateaux are difficult and ambiguous to identify in this case.

Finally we remark that we have also performed some matching calculations in $SU(3)$ at $\beta = 40.0$, which corresponds to about the same lattice spacing. The corresponding $f \otimes f \otimes \bar{f}$ irreducible representations are the 6 and 15. In both cases the energy plateaux are more ambiguous, particularly where we compare the 15 with the 120 of $SU(6)$. This may be due to the fact that certain mixings and decays are less suppressed for $SU(3)$ than for $SU(6)$.

5 Excited states: massive or stringy?

One of our motivations for studying flux tubes in higher representations is that we expect such bound states of fundamental flux tubes to have a low-lying excitation spectrum that contains clear signatures of the binding scale. This should provide an interesting contrast to the low-lying spectrum of fundamental flux tubes which, unexpectedly, shows no sign of the excitation of the massive modes that one would expect to be associated with an ‘intrinsic width’ for the flux tube. While one might question the existence of such an intrinsic width, the existence of a non-zero binding in the case of, say, the $2A$ flux tube is unambiguous. This would, most simply, reveal itself in extra excited states, representing massive rather than the usual stringy massless modes. Our cleanest spectra in this paper are for $k = 2A$ and $k = 3A$ so we shall focus on these. So does the $k = 2A$ $p = 0$ spectrum shown in Fig. 6 reveal any massive modes that are additional to the stringy excitations which, at large l , tend to the Nambu-Goto curves? (The same observations apply to the $k = 3A$ spectrum.) Since the low-lying excitation spectrum of fundamental flux tubes appears to contain only stringy states and no massive modes, it is interesting to compare our $k = 2A$ spectrum to the fundamental one shown in Fig.12 of [6]. The immediate question this comparison raises, as pointed out in our earlier study of $k = 2$ flux tubes in [7], is whether the first excited $k = 2A$ state might be a massive mode, with the second excited state being the first excited stringy mode and the next two $P = +$ excited states eventually tending to the second Nambu-Goto level? (We have not shown higher $P = +$ excited states in Fig. 6, but they are there.) Or it might be that the large deviations from Nambu-Goto are largely driven by the ‘unstable’ character of these flux tubes, and that otherwise the first excited state is much like the fundamental one. However this possibility appears to be contradicted by our results in this paper for the much more stable $k = 3A$ states, plotted in Fig. 16, which show similarly large deviations from the

Nambu-Goto predictions. Or again, it might be that we are seeing here the mixing of modes, enhanced by the existence of intermediate states that are not far from threshold. This could be the mixing of nearby stringy modes, or of a stringy mode with a massive mode - which would also imply the presence of an extra mode.

So we want to ask if the first excited states in the $k = 2A$ and $k = 1$ cases are the ‘same’ or not. It is of course not possible to answer this question unambiguously, and we choose to address it in the same way as we did in [7]. The idea is that if this state is indeed an approximate Nambu-Goto-like string excitation then we would expect its wavefunctional to have the appropriate ‘shape’. What that ‘shape’ should be, in terms of our highly blocked/smeared link matrices, is not at all evident, but it is something we do not need to know because we can simply compare it to the wavefunctional of the first excited $k = 1$ state, which we have good reason to think of as being stringy..

The way we make this comparison is as follows. Let $\{\phi_i; i = 1, \dots, n_o\}$ be our set of winding flux tube operators, with $P = +$ and $p = 0$. These operators are group elements, not yet traced, and may be in any representation of $SU(N)$. Suppose the flux is in the representation R . When we perform our variational calculation over this basis, we obtain a set of wavefunctionals, Φ_R^n , which are an approximation to the corresponding eigenfunctions of the Hamiltonian. Unfortunately we cannot simply compare $R = f$ and $R = 2A$ states by calculating their overlap: it will vanish because of the center symmetry. So instead we proceed as follows [7]. We write the wavefunctionals as linear combinations of our basis operators:

$$\Phi_R^n = \sum_i^{n_o} b_{R,i}^n c_{R,i} \text{Tr}_R(\phi_i) \equiv \sum_i^{n_o} b_{R,i}^n \text{Tr}'_R(\phi_i) \quad (18)$$

choosing the coefficients $c_{R,i}$ to satisfy the normalisation condition

$$\langle \text{Tr}'_R(\phi_i(0)) \text{Tr}'_R(\phi_i(0)) \rangle = 1 \quad (19)$$

so as to ensure that a comparison of the coefficients $b_{R,i}^n$ between different representations R can be meaningful. The idea is that the coefficients $b_{R,i}^n$ encode the ‘shape’ of the state corresponding to the wavefunctional, because they multiply the same operators, albeit in different representations, and with a common normalisation. So making the simple substitution

$$\Phi_{2A}^n = \sum_i^{n_o} b_{2A,i}^n \text{Tr}'_{2A}(\phi_i) \longrightarrow \tilde{\Phi}_{2A}^n = \sum_i^{n_o} b_{2A,i}^n \text{Tr}'_f(\phi_i) \quad (20)$$

we can compare our excited $k = 1$ and $k = 2A$ wavefunctionals by comparing $\tilde{\Phi}_{2A}^n$ with the fundamental wavefunctionals, Φ_f^n . This we can do by calculating the overlap

$$O_{n',n} = \frac{\langle \Phi^{n'\dagger}_f \tilde{\Phi}_{2A}^n \rangle}{\langle \Phi^{n'\dagger}_f \Phi_f^{n'} \rangle^{1/2} \langle \tilde{\Phi}_{2A}^{n\dagger} \tilde{\Phi}_{2A}^n \rangle^{1/2}} \quad (21)$$

(all operators at $t = 0$) which we assume provides us with a measure of the similarity between the original state Φ_{2A}^n and the state $\Phi_f^{n'}$.

Even if one accepts this method of comparison, there are some important caveats. The variational calculation is performed over a limited basis, so the Φ_f^n are only approximate energy eigenfunctionals. And the level of approximation will generally be different for different representations (and states). Thus the comparison is inevitably approximate. Again, we note that the operator basis ϕ_i varies with l (in lattice units). So we perform the comparison of f and $2A$ states at the same l . However ideally we should also compare at the same string tension i.e. at different lattice spacings such that $a\sqrt{\sigma_{2A}} = a'\sqrt{\sigma_f}$ and hence different β . Because of the additional costs we have not done so here, and this also makes the comparison approximate.

Given the approximate and heuristic nature of this method, we need to test it in a case where we are confident that we know the answer. This is the case for the absolute ground state. So in Fig. 29 we display the above overlaps of the variational ground states of the $k = 2A$ and adjoint flux tubes onto the lightest 20 fundamental variational eigenfunctionals, all on $l/a = 32$ lattices. In Fig. 30 we do the same on a $l/a = 64$ lattice. The result is clear-cut, both for stable and unstable flux tubes, and for both lengths: we observe that the method works very well in producing an almost exclusive overlap onto the f ground state. This is in fact representative of all our results for the absolute ground state, even where the state is unstable, and this gives us some confidence in this method.

We turn now to the $k = 2A$ $p = 0$ first excited state. In Fig. 31 we show the overlap of $\tilde{\Phi}_{2A}^{n=1}$ onto the lowest Φ_f^n , for $l/a = 32$ and $l/a = 64$ lattices. In Fig. 32 we do the same for the corresponding $k = 3A$ state. While the largest overlap is indeed on the first excited fundamental state, there is also a small but visible overlap onto the 2nd excited stringy f state, $\Phi_f^{n=2}$, and this is very similar for the $k = 2A$ and $k = 3A$ states and for both flux tube lengths. While the comparison is not as unambiguous as for the ground state, it is hard to avoid the conclusion that this state is definitely not some new massive mode excitation. Rather it appears to be largely the first excited stringy mode, with a modest admixture of the second. The shift in energy away from Nambu-Goto might be largely the result of this mixing. We also note that the mixing appears to become smaller as l increases from $l/a = 32$ to $l/a = 64$ and the energy approaches that of the Nambu-Goto prediction. We remark that all this confirms that the first excited state at lower l does indeed asymptote to the first excited Nambu-Goto energy level, and does not cross the latter somewhere between $l/a = 52$ and $l/a = 64$ – an alternative possibility that we discussed earlier, in Section 4.2, when considering Fig. 6.

It is interesting to contrast this with what one finds for the 2nd and 3rd excited states in the $k = 2A, 3A$ and $p = 0, P = +$ sectors. Typical examples are shown in Figs. 33 and 34. Here it is hard to draw any conclusion. While the dominant overlap is onto the corresponding fundamental excited state, there is a large projection on other states as well. It certainly appears possible that some new massive mode either dominates or is mixed into one or both of these states.

6 Discussion and conclusions

In this paper we have calculated the low-lying spectrum of closed flux tubes in various representations, with the length of the flux tube stabilised by closing it around a spatial torus. We had several motivations for this study.

One is to compare the resulting spectrum to simple effective string actions, just as we did in our earlier work on fundamental flux tubes [6]. Since higher representation flux tubes can be thought of as bound states of (anti)fundamental flux tubes, the massive excitation modes associated with that binding should leave a signature in the spectrum. In the case of fundamental flux tubes we found no trace at all of massive non-stringy modes and our hope was to find something different here.

Of course only a few of these flux tubes are stable against decay and are real bound states. Recall that only some decays are large- N suppressed by large- N counting arguments. For example the decay of an adjoint flux tube to the vacuum (plus glueballs) is suppressed at $N = \infty$, but its decay into a pair of noninteracting fundamental and anti-fundamental flux tubes need not be, since $\text{Tr}_{\text{adj}} l_p = \text{Tr}_f l_p \text{Tr}_f^\dagger - 1$. (Although the dynamics may of course suppress such decays.) Most higher representation ‘flux tubes’ are unstable at large N , in this sense, and it is not a priori clear if they exist in the same way as unstable ‘resonant’ particle states exist. While there is evidence for the existence of such flux tubes when attached to appropriate sources [19], their stability in that case is usually ensured (for the relevant length scales) by the fact that screening the sources by gluons costs extra energy. Our closed flux tubes are not protected from being screened, and decaying, in this way. So one of the things we wished to learn is which of the unstable flux tubes were stable enough that one could analyse them by conventional methods, and which needed new methods and what those new methods might be.

A closely related question is whether it makes sense to classify flux tubes according to the irreducible representations of $\text{SU}(N)$, given that the vacuum contains adjoint gluons that can screen and mix the representations of sources and flux tubes. Earlier calculations have provided evidence that this is indeed the case for k -strings [8, 7], and in Table 7 we have provided similar evidence for all the representations being considered here. Apart from finite volume effects (both in the transverse size and in l) the screening appears to be (almost?) exact. Why this should be so, at what is not a very large value of N , is an interesting puzzle that is being investigated by us, more systematically, elsewhere [20].

Our first conclusion, discussed in Section 4, is that the absolute ground state and the lightest states with non-zero longitudinal momenta are accurately described by the free string expression in eqn(3) all the way down to our lowest values of l , which are very close to the minimal possible flux tube length at $l = 1/T_c$. This is clearest for the very stable flux tubes in the $k = 2A$ and $k = 3A$ representations, which are our most accurate calculations (see Figs 2 and 14) but it is also the case, within larger errors, for all representations, including flux tubes that could be very unstable. (See Figs.9, 18, 20, 22, 26, 28 for the 2S, 3M, 3S, adjoint, 84, and 120 representations respectively.) This is of course just what has been observed for the corresponding fundamental flux tube states in [6].

In the case of the $p = 0$ ground state the stringy corrections are small all the way down

to $l\sqrt{\sigma} \sim 1$ (basically because they arise from the zero-point energies) and so an expansion of the energy in powers of $1/l\sqrt{\sigma}$ is convergent over our whole range of l . So it is fair to claim that the close agreement we are seeing with Nambu-Goto down to small values of $l\sqrt{\sigma}$ is a prediction of the known universal corrections to the linear σl piece [3, 12, 11, 10] – at least when the flux tube is stable. In fact, as discussed in Section 4.2, what we are able to confirm, within our statistical errors, is the presence of the linear piece and, in some cases, the $-\pi/6l$ universal Lüscher correction, but not really any more than that. (See e.g. Fig. 3.) Our most accurate spectra, for the $k = 2A$ and $k = 3A$ representations, allowed us to confirm the universal value of this coefficient at the $\pm 10\%$ level, which is a usefully accurate result for these bound-state flux tubes.

The $p \neq 0$ ground states are another matter. Here we can confirm, in some cases very accurately, the excitation energy $= |p|$ of the massless excitation that carries the momentum on the background flux tube, as shown in Figs. 4, 10, 23 for the $2A$, $2S$ and adjoint flux tubes respectively. In fact our calculations are accurate enough to confirm the presence of the additional zero-point energy, as discussed in Section 4.2 and displayed in Fig. 4. Indeed we saw that in any non-stringy attempt to describe these spectra, the particle excitation carrying the non-zero momentum will have a mass that is constrained by our calculated spectrum to be very much smaller than the known mass gap of the bulk space-time theory [23, 24]. Thus such a (presumably massless) excitation must exist on the flux tube rather than in the bulk, and will thus arise from an effective string action.

That we observe a (near) free-string behaviour, even when the flux tube is very short, is more surprising for the $p \neq 0$ ground states than for the $p = 0$ ground state. This is because the expansion in powers of $1/l\sqrt{\sigma}$ diverges at quite large l for $p \neq 0$, so we cannot use universality arguments to predict the $p \neq 0$ spectrum at small l in the way we could for $p = 0$. All this parallels what has previously been seen for the fundamental flux tube [6]. There we suggested [6] that what these ground states have in common is that they all have a phonon content that is either all left moving or all right moving, so that all phonon subenergies are at threshold and it is plausible that the interaction of these Goldstone bosons will vanish there, removing at least one possible source of corrections to the free-string result. We note that a very recent and much more complete analysis of phonon scattering in a finite volume comes to a similar conclusion [14]. Our results here, with higher representation flux tubes, are consistent with this picture. We also remark that, as shown in Fig. 2, a ‘minimalist’ model where the ground state with $p \neq 0$ consists of a $p = 0$ flux tube together with massless noninteracting particles sharing p , gives predictions very close to Nambu-Goto. (In contrast to a large discrepancy for other states that involve both right and left movers.) It may thus be that, to a first approximation, this part of the spectrum is independent of the model used (within limits). But this is only a speculation.

By contrast other states, for example the $p = 0$ excited $k = 2A$ and $k = 3A$ states shown in Figs 6 and 16, show very large deviations from Nambu-Goto, making it hard to say to what extent that model provides any kind of first approximation to this part of the spectrum. We recall that in the case of fundamental flux tubes the corresponding corrections are significant but small, with a rapid approach to the free-string spectrum as $l \uparrow$ [6]. There are two obvious differences between the fundamental flux tube and the ones here. Firstly, here we have a

binding dynamics which may perturb the spectrum through its excitations. Secondly most of the states are not only unstable at finite N but remain so in the $N \rightarrow \infty$ limit. If mixing is the dominant effect, then the states will contain non-stringy components, while if instability is the dominant effect then they will be stringy but resonance-like. In this context we note that at the larger values of l in Fig.16, the lightest $p = 0$ excited states become stable, in contrast to the case of $k = 2A$ shown in Fig.6. Nonetheless the deviations from Nambu-Goto are not significantly different in the two cases. This suggests that instability is not the main reason for the large deviations we see for the second excited state at these values of l .

The striking difference between the simple stringy behaviour of the $p \neq 0$ ground states, even when these are unstable, and the messy behaviour of the unstable excited states may be due to the fact that in the former case, unlike the latter, the phonons will not catalyse the decay of the flux tube because they have zero subenergies [4]. Although this may not be the only source of flux tube decay, it may be a significant factor.

To make some progress in identifying the nature of the $p = 0$ excited states we introduced in eqns(18-21) a heuristic measure [7] for comparing states in different representations. Applied to the $p = 0$ ground states it confirmed unequivocally that these are just the same as the unexcited flux tube in the fundamental ground state, and that this is so for all the representations we consider here. See for example Figs 29 and 30 for the $k = 2A$ and adjoint cases. This is as expected, and motivates the use of the measure for the more controversial excited states. For the first excited $k = 2A$ $p = 0$ state, as shown in Fig. 31, the result is less unequivocal but points to it being quite similar to the corresponding fundamental state and becoming more so as $l \uparrow$. We note that what we show in the figures is the overlap-squared, whereas it is possible that the energy shift contains pieces proportional to the overlap, which is larger and could produce a significant shift in the energy. For the second and third excited $p = 0$ states, analysed in Figs 33 and 34, we see states that are very unlike the corresponding fundamental ones. This suggests that while the ground and first excited $p = 0$ states in Fig. 6 are indeed (mostly) stringy, the higher states may well include a large admixture with massive modes.

Because nearly all our states are unstable, it is important to approach our energy estimates as critically as possible, and we have attempted to do so. (At the risk of being tedious.) One usually obtains an energy from a correlation function by calculating the effective energy, $aE_{eff}(t) = -\ln C(t+a)/C(t)$, and identifying a ‘plateau’ for $t \geq t_0$ where t_0 has to be small if the result is to be usefully accurate. The stable $k = 2A, 3A$ $p = 0$ ground states provide our benchmark for an unambiguous calculation, as shown in Figs 1, 15. As $l \uparrow$ the energy increases $\propto l + O(1/l)$ and the signal, $\sim \exp\{-aE(l)n_t\}$, drops into the statistical noise at smaller $t = an_t$, so decreasing the useful extent of the plateau. Apart from this there is no ambiguity in extracting energies. The $p \neq 0$ ground states are similar, although the energies are larger so, once again, reducing the useful energy plateau. States that are unstable but with a small decay width should, by continuity, produce a plateau at intermediate t , which eventually sinks to the decay threshold. (As long as we remain within the same limited class of operators that are designed to project onto single flux tubes.) If the decay width is large, we will lose all sign of a plateau. Examples of the former are the adjoint ground state in Figs 24 and 25 and, less stable, the $k = 2S$ ground state in Fig. 11. A totally unstable state

is the first excited $k = 2S$ $p = 0$ state shown in Fig. 12. For obvious reasons we have not attempted to extract an energy for this state. This is to be contrasted with the first excited $k = 2A$ $p = 0$ state which we show in Fig. 7. While there is no plateau for $l/a = 16$, one can just about attempt to discern one for $l/a = 20$ and more easily for higher l . We attempted heuristic unstable particle fits to such effective masses, using decay channels weighted with a Breit-Wigner for the unstable state as in eqn(16). Examples are in Fig. 8 and Fig. 13. The interesting feature of such fits is that the true energy is not to be found by looking at $E_{eff}(t)$ at large t , but is typically close to the value of $\lim_{t \rightarrow 0} E_{eff}(t)$ i.e. it is very much larger. This could significantly reduce the large discrepancy between Nambu-Goto and our observed $p = 0$ excited states. This highlights the dangers in using conventional methods to make energy estimates when the state is not stable or very nearly so.

Despite our uncertainty concerning the existence of many of the excited states, the existence of the absolute ground states, whether stable or unstable, appears to be quite unambiguous. And this is often also true of the ground states with $p \neq 0$. Moreover even when the flux is in our rather exotic representations, these particular states have the simple stringy excitations of a free string theory, even as l decreases close to its physically minimum value. The spectrum of other excited states is more complex and there appears to be plenty of room there for the massive modes that might arise from the binding energy in these states.

Acknowledgements

During the course of this work, MT participated in the *Recent Advances in Numerical Methods for Field Theory and Gravity* Workshop at the KITP, Santa Barbara, and in the *New Frontiers in Lattice Gauge Theory* Workshop at the Galileo Galilei Institute, Florence, and acknowledges useful discussions with a number of participants. Part of this work was also done during the *Large- N gauge theories* Workshop at the Galileo Galilei Institute, Florence, and AA and MT would like to thank the organisers for the warm hospitality and many of the participants for useful discussions. This paper is a continuation of a project whose earlier stages were in collaboration with Barak Bringoltz whom we thank, with pleasure, for his role in helping to develop many of the ideas and techniques used in this paper. The computations were carried out on computers in Oxford Theoretical Physics funded by EPSRC and Oxford University.

A Representations and Casimirs

In this Appendix we describe in detail how to calculate flux tubes in the representations of interest to us in this paper, and how to determine some of their group theoretic properties.

Consider a Polyakov loop

$$l_p = \prod_{n_x=1}^{n_x=L_x} U_x(n_x) \quad (22)$$

that winds once around the (spatial) x -torus of length L_x in lattice units. (We suppress other co-ordinates.) If we take the trace in the representation R , then the operator $\text{Tr}_R\{l_p\}$ is a candidate operator for projecting onto winding flux tubes carrying flux in the representation R . One can deform the Polyakov loop in eqn(22) so as to obtain winding operators that can be used to form flux tubes with non-trivial quantum numbers. These operators can be used as a basis for a variational calculation of the spectrum as described in the text. We use here the same basis as we used for the fundamental flux tube in [6], and we refer to that paper for a list of the operators.

The open version of such a flux tube would connect sources in the representations R and \bar{R} . But because the vacuum contains gluons a flux tube in representation R may evolve into one in R' by gluon screening if R and R' can be connected by a product of adjoints. And of course a flux tube in R may evolve into a product of flux tubes carrying fluxes R_1, R_2, \dots if R appears in the product $R_1 \otimes R_2 \otimes \dots$. Equally an excited flux tube may decay into a lower lying flux tube of the same representation plus colour singlet glueballs. The same remarks apply to a closed flux tube winding around the spatial torus. In most cases such a flux tube will not be absolutely stable and whether it exists at all, in the sense that an unstable but narrow resonance exists, will depend on the dynamics.

Note that some decays will be suppressed by the usual ‘kinematic’ large- N counting arguments, for example the decay of a sufficiently excited flux tube state into its ground state together with a glueball. Other decays are not suppressed in this way, e.g. the decay of an adjoint flux tube into a pair of fundamental and anti-fundamental flux tubes. (Although it may be that the detailed dynamics suppresses such a decay.) The latter is analogous to the expected ‘falling apart’ as $N \rightarrow \infty$ of a molecular hadronic state (such as, perhaps, the inverted nonet scalars at $\leq 1\text{GeV}$), while the former is analogous to the ρ meson becoming stable in that limit.

Consider the fundamental representation f . Any representation R will appear in a product of a number of f and \bar{f} . Suppose that the number of these is N_f and $N_{\bar{f}}$ respectively, then we define the \mathcal{N} -ality of the representation to be

$$k = N_f - N_{\bar{f}}. \quad (23)$$

and we use the generic name of a ‘ k -string’ for such a flux tube. The reason for focusing on the \mathcal{N} -ality is that for an $\text{SU}(N)$ gauge theory k is conserved (module N) under gluon screening (since gluons are adjoints carrying $k = 0$). So for $N \geq 4$ the lightest $k = 2$ flux tube is an absolutely stable state, as is the lightest $k = 3$ flux tube for $N \geq 6$. Of course it may be that such a $k = 2$ ‘flux tube’ consists of nothing more than two $k = 1$ flux tubes. Whether it does

or not is a dynamical question which, in fact, has been answered (see e.g. [16, 8]), and we know that the lightest $k = 2$ and $k = 3$ strings are flux tubes in their own right, which are strongly bound, stable states in $SU(6)$ [8].

The irreducible representations we consider in this paper include the totally anti-symmetric and symmetric of $f \otimes f$ (referred to as $k = 2A$ and $k = 2S$), and the anti-symmetric, mixed and symmetric of $f \otimes f \otimes f$ (referred to as $k = 3A$, $k = 3M$ and $k = 3S$). The construction and properties of these are obtained in the Appendices of [16] to which we refer the reader for details, in particular for the derivation of the appropriate operators, and for the values of the quadratic Casimir,

$$C_2(R) = \text{Tr}_R T^a T^a \quad (24)$$

where R is the representation and the T^a are the generators of the group.

We also consider in this paper the following representations: the adjoint, which is $k = 0$ and is the non-singlet piece of $f \otimes \bar{f}$, and the 84 and 120 which are both $k = 1$ and which arise in $f \otimes f \otimes \bar{f}$. These are the representations we shall now describe in more detail.

A standard and efficient method for dealing with the representations of $SU(N)$ is Young tableaux. For the derivation and rules of use we refer to [25]. We will label a tableau by $Y(\lambda_1, \lambda_2, \dots)$ where λ_i is the number of boxes in the i 'th row of the tableau. We recall the rule that $\lambda_i \geq \lambda_{i+1}$, and we only show the λ_j for rows j containing at least one box. So, for example, f corresponds to $Y(\lambda_1 = 1)$, \bar{f} corresponds to $Y(\lambda_1 = 1, \lambda_2 = 1, \dots, \lambda_{N-1} = 1)$, while the adjoint is given by $Y(\lambda_1 = 2, \lambda_2 = 1, \dots, \lambda_{N-1} = 1)$. We also recall that the dimension d_R of the representation R corresponding to the tableau $Y(\lambda_1, \lambda_2, \dots)$ is given by [25]

$$d_R = \frac{\prod_{i < j}^N (l_i - l_j)}{(n-1)!(n-2)! \dots 1!} \quad ; \quad l_k = \lambda_k + N - k, \quad k = 1, \dots, N \quad (25)$$

and that its quadratic Casimir is given by [16]

$$C_2(R) = \frac{1}{2} \left(n_b N + \sum_{i=1}^{n_r} \lambda_i (\lambda_i + 1 - 2i) - \frac{n_b^2}{N} \right). \quad (26)$$

where $n_b = \lambda_1 + \lambda_1 + \dots$ is the total number of boxes in the tableau and n_r is the number of rows.

Applying eqns(25,26) to the fundamental tableau, $Y(\lambda_1 = 1)$, gives

$$d_f = N \quad ; \quad C_2(f) = \frac{N^2 - 1}{2N} \quad (27)$$

The adjoint representation is obtained from $f \otimes \bar{f} = \underline{1} + \underline{adj}$. The singlet corresponds to adding the single f box to the bottom of the \bar{f} column of boxes, while the adjoint is obtained by adding it to the first row. Applying eqns(25,26) to the resulting adjoint tableau, $Y(\lambda_1 = 2, \lambda_2 = 1, \dots, \lambda_{N-1} = 1)$, gives

$$d_{adj} = N^2 - 1 \quad ; \quad C_2(adj) = N \quad (28)$$

For $SU(6)$ we see that $d_{adj} = 35$.

Consider now the product $\bar{f} \otimes f \otimes f$. As we saw above the first product gives us $\bar{f} \otimes f = \underline{1} + \underline{adj}$. Adding the second f box to the singlet just gives us an f again, while adding it to the adjoint $Y(\lambda_1 = 2, \lambda_2 = 1, \dots, \lambda_{N-1} = 1)$ gives us $R_a = Y(\lambda_1 = 3, \lambda_2 = 1, \dots, \lambda_{N-1} = 1)$ if we add it to the first row and $R_b = Y(\lambda_1 = 2, \lambda_2 = 2, \lambda_3 = 1, \dots, \lambda_{N-1} = 1)$ if we add it to the second, as well as a second f by adding it to the bottom of the first long column (which is then of length N and so can be dropped). Applying eqns(25,26) to these tableaux gives,

$$d_{R_a} = \frac{1}{2}N(N+2)(N-1) \quad ; \quad C_2(R_a) = \frac{(3N-1)(N+1)}{2N} = C_2(f) \frac{3N-1}{N-1} \quad (29)$$

and

$$d_{R_b} = \frac{1}{2}N(N+1)(N-2) \quad ; \quad C_2(R_b) = \frac{(3N+1)(N-1)}{2N} = C_2(f) \frac{3N+1}{N+1}. \quad (30)$$

For $SU(6)$ we can label these representations by their dimensions, i.e.

$$R_a = \underline{120} \quad ; \quad R_b = \underline{84} \quad : \text{ for } SU(6) \quad (31)$$

and evaluating the quadratic Casimirs we obtain the entries in Table 2.

To calculate the spectrum of a flux tube in representation R we want correlators of operators $\text{Tr}_R l_p$ where l_p is some loop winding (once) around the appropriate spatial torus, the simplest example being that in eqn(22). Since our Monte Carlo generates group elements U_l that are in the fundamental representation, we need to express $\text{Tr}_R l_p$ in terms of $\text{Tr}_f l_p$. This can be done by taking products of group elements and imposing the (anti)symmetry constraints on the indices that are encoded in the corresponding Young tableaux, as carried out explicitly in [16] for the $2A, 2S$ and $3A, 3M, 3S$ representations. Often we can employ a short cut. For example if we want R and we find that $R_1 \otimes R_2 = R_3 \oplus R$ then we can use the fact that $\text{Tr}_{R_1} l \times \text{Tr}_{R_2} l = \text{Tr}_{R_3} l + \text{Tr}_R l$. For example, we know that the adjoint satisfies $f \otimes \bar{f} = \underline{adj} \oplus \underline{1}$ (where $\underline{1}$ is the singlet) so

$$\text{Tr}_{adj} l = \text{Tr}_f l \text{Tr}_{\bar{f}} l - 1 = |\text{Tr}_f l|^2 - 1. \quad (32)$$

We also want such an expression for the representations R_a and R_b . One can easily see that $2S \otimes \bar{f} = R_a \oplus f$ giving

$$\text{Tr}_{R_a} l = \text{Tr}_{2S} l \text{Tr}_f l^\dagger - \text{Tr}_f l = \frac{1}{2} (\text{Tr}_f^2 l + \text{Tr}_f l^2) \text{Tr}_f l^\dagger - \text{Tr}_f l \quad (33)$$

and that $2A \otimes \bar{f} = R_b \oplus f$ giving

$$\text{Tr}_{R_b} l = \text{Tr}_{2A} l \text{Tr}_f l^\dagger - \text{Tr}_f l = \frac{1}{2} (\text{Tr}_f^2 l - \text{Tr}_f l^2) \text{Tr}_f l^\dagger - \text{Tr}_f l \quad (34)$$

where we use the fact that $\text{Tr}_{\bar{f}} l = \text{Tr}_f l^\dagger$ and we obtain $\text{Tr}_{2S, 2A} l$ from [16]. The above expressions are for general N and for $SU(6)$ give us the appropriate operators for the adjoint, $\underline{120}$ and $\underline{84}$ respectively.

References

- [1] M. Lüscher, K. Symanzik and P. Weisz, Nucl. Phys. B173 (1980) 365.
M. Lüscher, Nucl. Phys. B180 (1981) 317.
- [2] J. Polchinski and A. Strominger, Phys. Rev. Lett. 67 (1991) 1681.
- [3] O. Aharony and Z. Komargodski, arXiv:1302.6257.
- [4] A. Monin and M.B. Voloshin, Annals Phys. 325 (2010) 16 [arXiv:0904.1728];
arXiv:0902.0407; Phys. Rev. D78 (2008) 125029 [arXiv:0809.5286]; Phys. Rev. D78 (2008)
065048 [arXiv:0808.1693].
- [5] M. Shifman and A. Yung, Phys. Rev. D66 (2002) 045012 [arXiv:hep-th/0205025].
A. Armoni and M. Shifman, Nucl.Phys. B671 (2003) 67-94 [arXiv:hep-th/0307020].
S. Bolognesi, M. Shifman and M.B. Voloshin, Phys.Rev. D80 (2009) 045010
[arXiv:0905.1664].
- [6] A. Athenodorou, B. Bringoltz and M. Teper, JHEP 1105 (2011) 042 [arXiv:1103.5854].
- [7] A. Athenodorou, B. Bringoltz and M. Teper, JHEP 0905 (2009) 019 [arXiv:0812.0334].
- [8] B. Bringoltz and M. Teper, Phys. Lett. B663 (2008) 429 [arXiv:0802.1490].
- [9] J. Arvis, Phys. Lett. 127B (1983) 106.
- [10] M. Lüscher and P. Weisz, JHEP 0407 (2004) 014 (arXiv:hep-th/0406205).
- [11] J. Drummond, arXiv:hep-th/0411017.
- [12] O. Aharony, M. Field and N. Klinghoffer, JHEP 1204 (2012) 048 [arXiv:1111.5757]
O. Aharony and M. Dodelson, JHEP 1202 (2012) 008 [arXiv:1111.5758]
O. Aharony and N. Klinghoffer, JHEP 1012 (2010) 058 [arXiv:1008.2648].
O. Aharony and M. Field, JHEP 1101 (2011) 065 arXiv:1008.2636.
O. Aharony and E. Karzbrun, JHEP 0906 (2009) 012 [arXiv:0903.1927].
- [13] F. Gliozzi and M. Meineri, arXiv:1207.2912.
M. Billo, M. Caselle, F. Gliozzi, M. Meineri and R. Pellegrini, JHEP 05 (2012) 130
[arXiv:1202.1984].
H. Meyer, JHEP 0605 (2006) 066 [arXiv:hep-th/0602281].
- [14] S. Dubovsky, R. Flauger and V. Gorbenko, arXiv:1301.2325.
- [15] S. Dubovsky, R. Flauger and V. Gorbenko, arXiv:1203.1054; arXiv:1205.6805.
- [16] B. Lucini and M. Teper, Phys. Rev. D64 (2001) 105019 [arXiv:hep-lat/0107007]; Phys.
Lett. B501 (2001) 128 [arXiv:hep-lat/0012025].
L. Del Debbio, H. Panagopoulos, P. Rossi and E. Vicari, Phys. Rev. D65 (2002) 021501
[arXiv:hep-th/0106185].

- [17] B. Lucini, M. Teper and U. Wenger, JHEP 0406 (2004) 012 [arXiv:hep-lat/0404008].
- [18] D. Karabali, C. J. Kim and V. P. Nair, Phys. Lett. B434 (1998) 103 [arXiv:hep-th/9804132].
D. Karabali, V. P. Nair and A. Yelnikov, Nucl. Phys. B824 (2010) 387 [arXiv:0906.0783].
- [19] S. Deldar, Phys. Rev. D62 (2000) 034509 [arXiv:hep-lat/9911008]; JHEP 0101 (2001) 013 [arXiv:hep-ph/9912428]; Eur. Phys. J. C47 (2006) 163 [arXiv:hep-lat/0607025].
G. Bali, Phys. Rev. D62 (2000) 114503 [arXiv:hep-lat/0006022].
- [20] A. Athenodorou and M. Teper, in progress.
- [21] H. Meyer and M. Teper, JHEP 0412 (2004) 031 [arXiv:hep-lat/0411039].
- [22] M. Teper, Phys. Lett. B183 (1987) 345; B185 (1987) 121.
- [23] B. Lucini and M. Teper, Phys. Rev. D66 (2002) 097502 [arXiv:hep-lat/0206027].
- [24] M. Teper, Phys.Rev. D59 (1999) 014512 [arXiv:hep-lat/9804008].
- [25] C. Itzykson and M. Nauenberg, Rev. Mod. Phys. 38 (1966) 95.

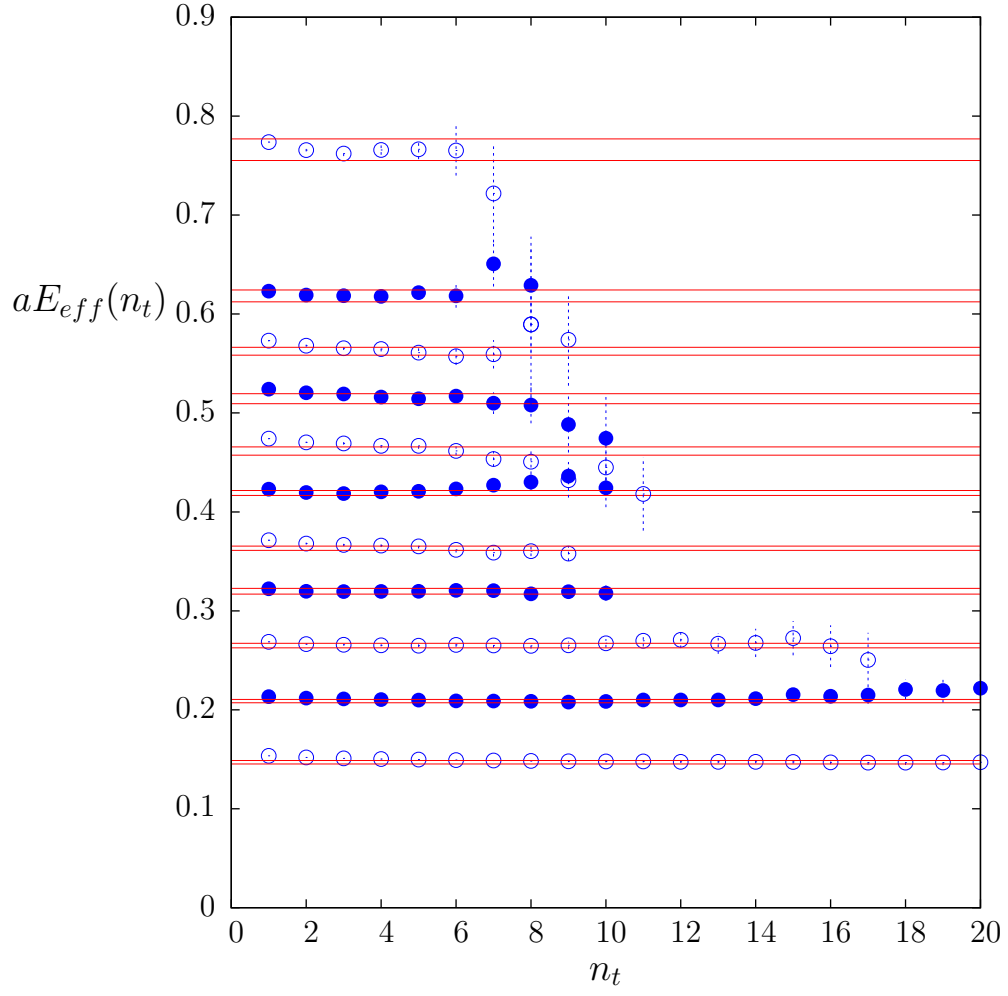


Figure 1: Effective energy of the $k=2A$, $p=0$, $P=+$ (variational) ground state of a flux tube of length $l/a = 16, 20, 24, 28, 32, 36, 40, 44, 48, 52, 64$. Lines are our plateaux estimates ($\pm 1\sigma$ error bands).

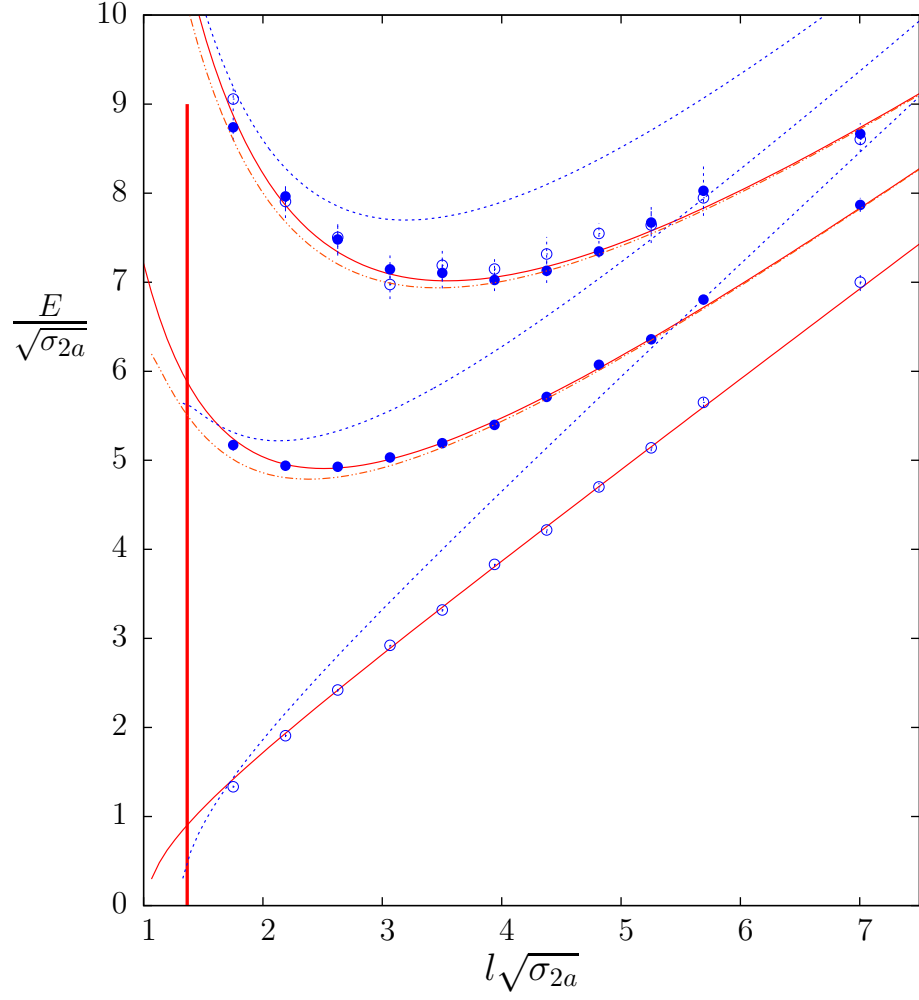


Figure 2: $k = 2A$ ground states with $p = 0, 2\pi/l, 4\pi/l$ and with $P = +, \circ$, and $P = -, \bullet$. Solid red curves are Nambu-Goto predictions. Dashed red lines are the model in eqn(15). Dashed blue lines denotes lower boundaries of scattering states formed of two fundamental flux tubes with total momentum p . Vertical line denotes location of ‘deconfinement’ transition.

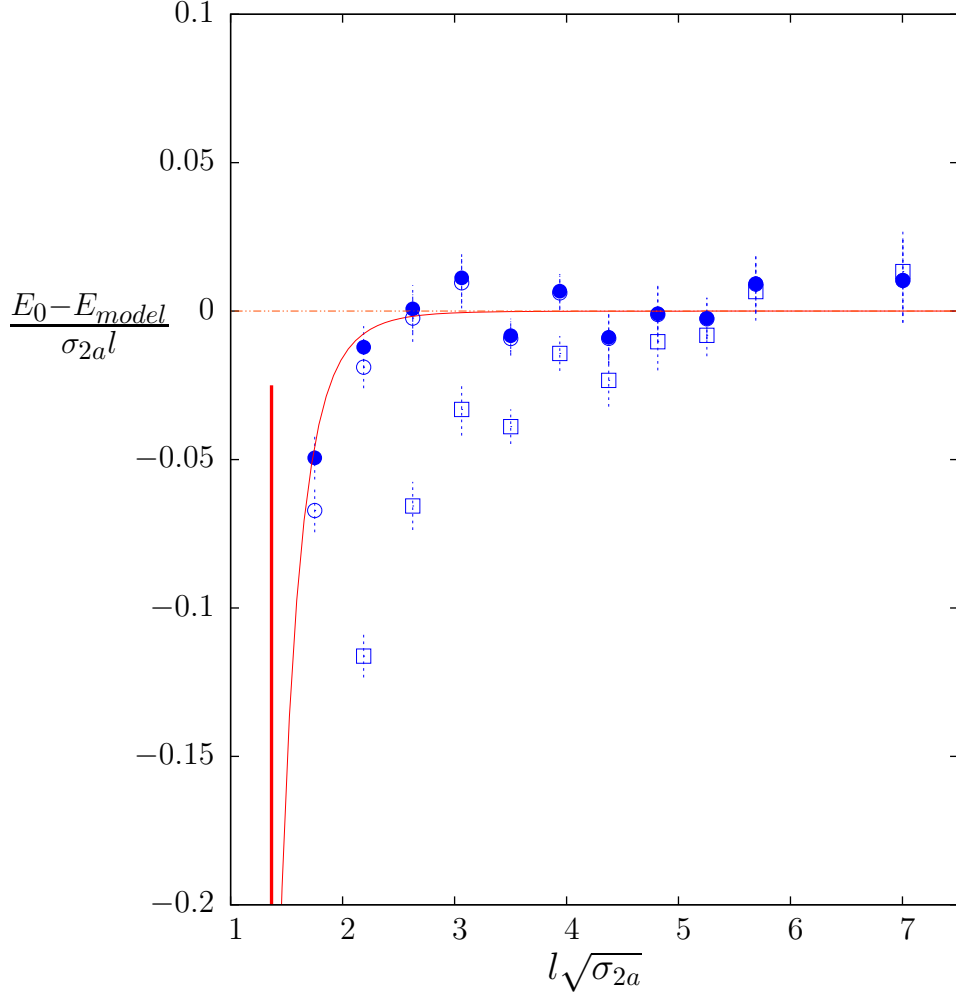


Figure 3: Energy of $k = 2A$ ground state with $p = 0$ and $P = +$, minus predictions of various ‘models’: Nambu-Goto, \bullet ; linear plus Lüscher correction, \circ ; and only linear term, \square . The solid curve includes an $O(1/l^7)$ correction to Nambu-Goto. Vertical line denotes location of ‘deconfinement’ transition.

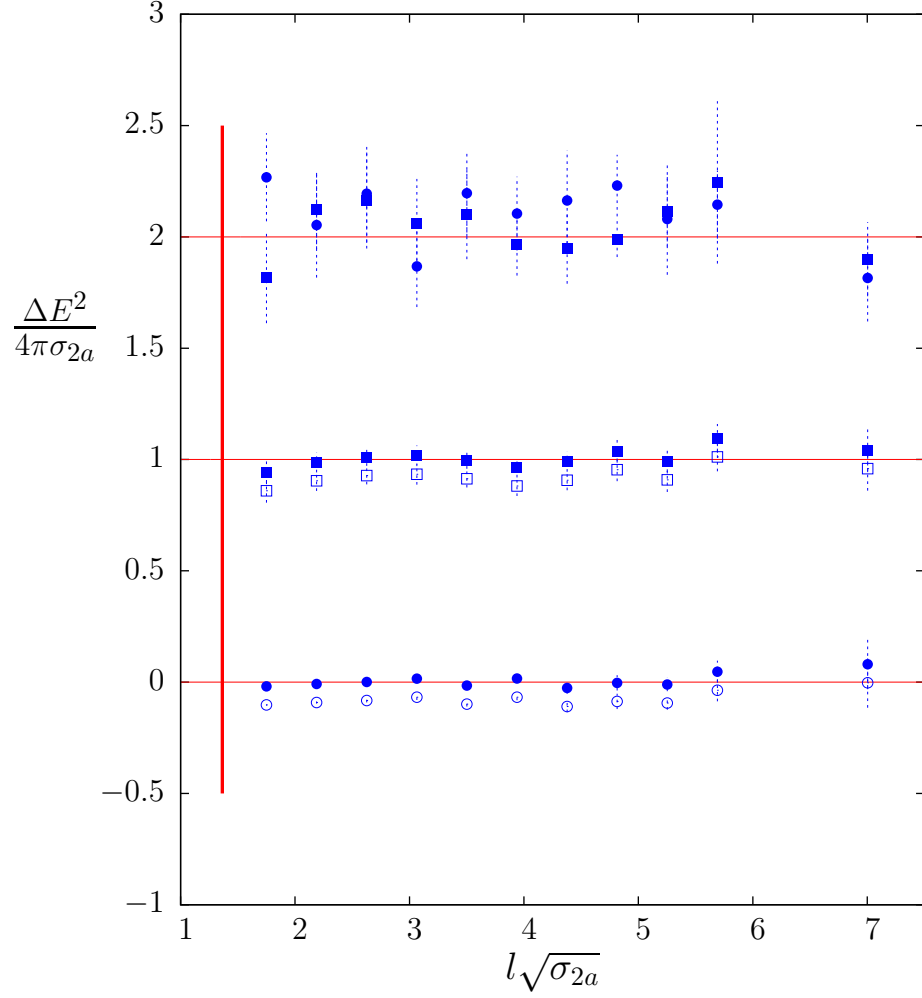


Figure 4: Phonon excitation energies, as defined in eqn(14), of $k = 2A$ ground states with $p = 0, 2\pi/l, 4\pi/l$ and with $P = +$ (\bullet) or $P = -$ (\blacksquare). Open symbols shown for $p = 0, 2\pi/l$ are without the zero-point energy in eqn(14). Horizontal lines are Nambu-Goto predictions. Vertical line denotes location of ‘deconfinement’ transition.

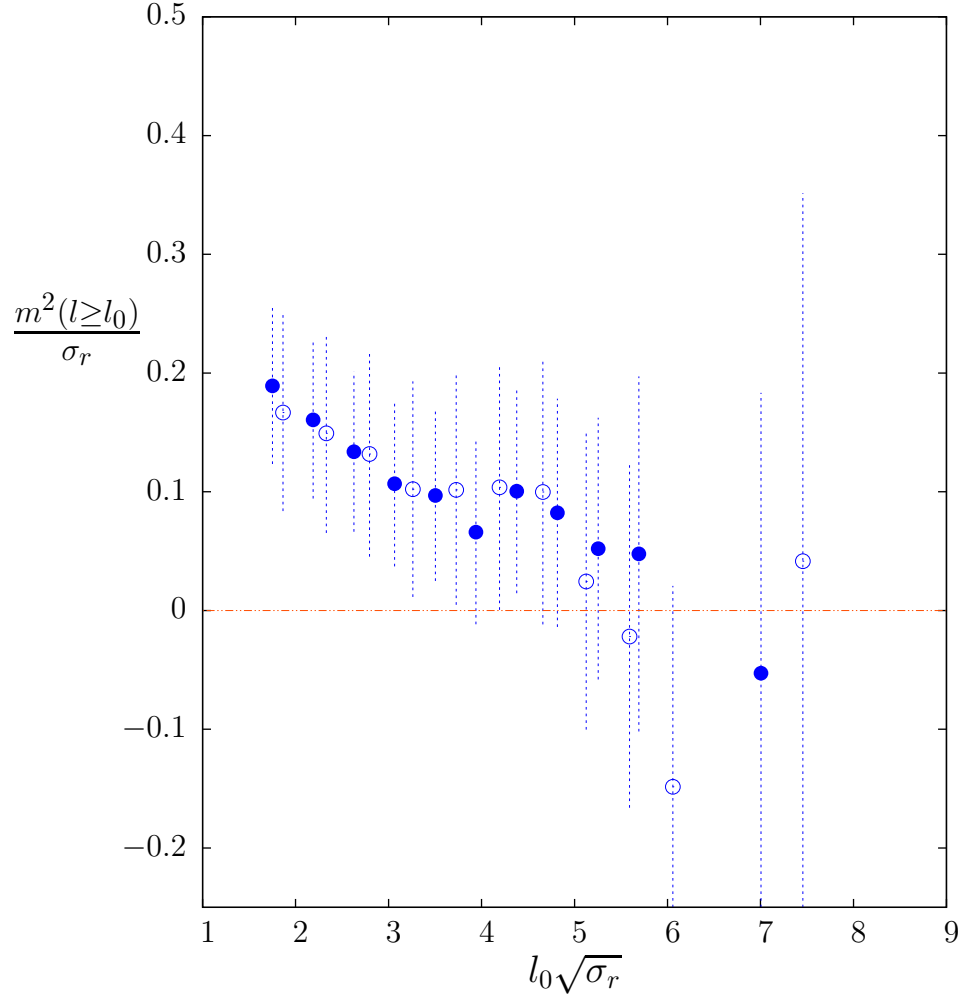


Figure 5: Fitting the $p = 2\pi/l$ ground state energies to the model in eqn(15) and extracting the excitation mass averaged over $l \geq l_0$. For representations $r = 2A$ (\bullet) and $r = 3A$ (\circ).

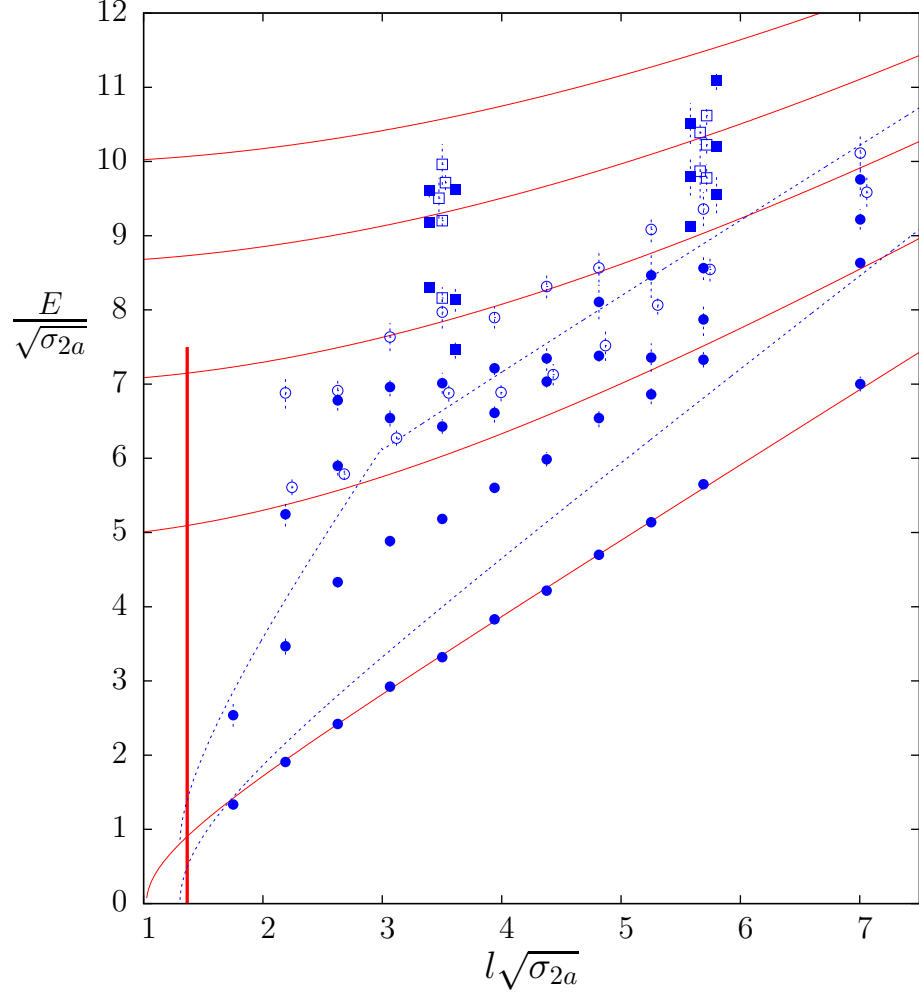


Figure 6: Energies of lightest $k = 2A$ $p = 0$ states with $P = +$, \bullet , and with $P = -$, \circ . Solid curves are corresponding Nambu-Goto levels. Upper dashed line is (approximately) the energy of the lightest $P = +$ decay channel consisting of a flux tube and glueball; lower line is that of two fundamental flux loops. Vertical line denotes location of ‘deconfinement’ transition.

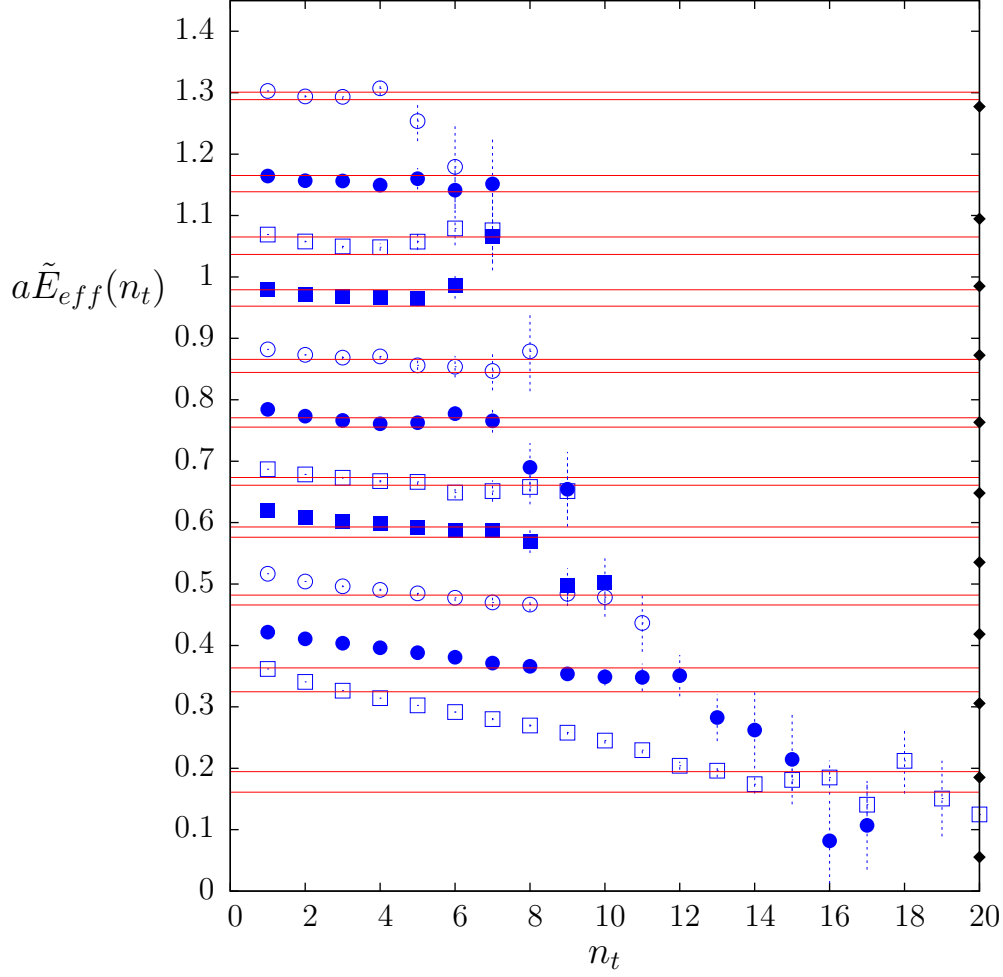


Figure 7: Effective energy, E_{eff} , of the $k=2A$, $p=0$, $P=+$ (variational) first excited state of a flux tube of length $l/a = 16, 20, 24, 28, 32, 36, 40, 44, 48, 52, 64$. Values shown have been shifted by multiples of 0.05 for clarity, $a\tilde{E}_{eff} = aE_{eff} + 0.05 * (l/a - 24)/4$, and a shift of 0.35 for $l = 64a$. Lines are $\pm 1\sigma$ error bands of our mean plateaux estimates. Points on right axis are corresponding decay thresholds ($= 2E_f(l)$).

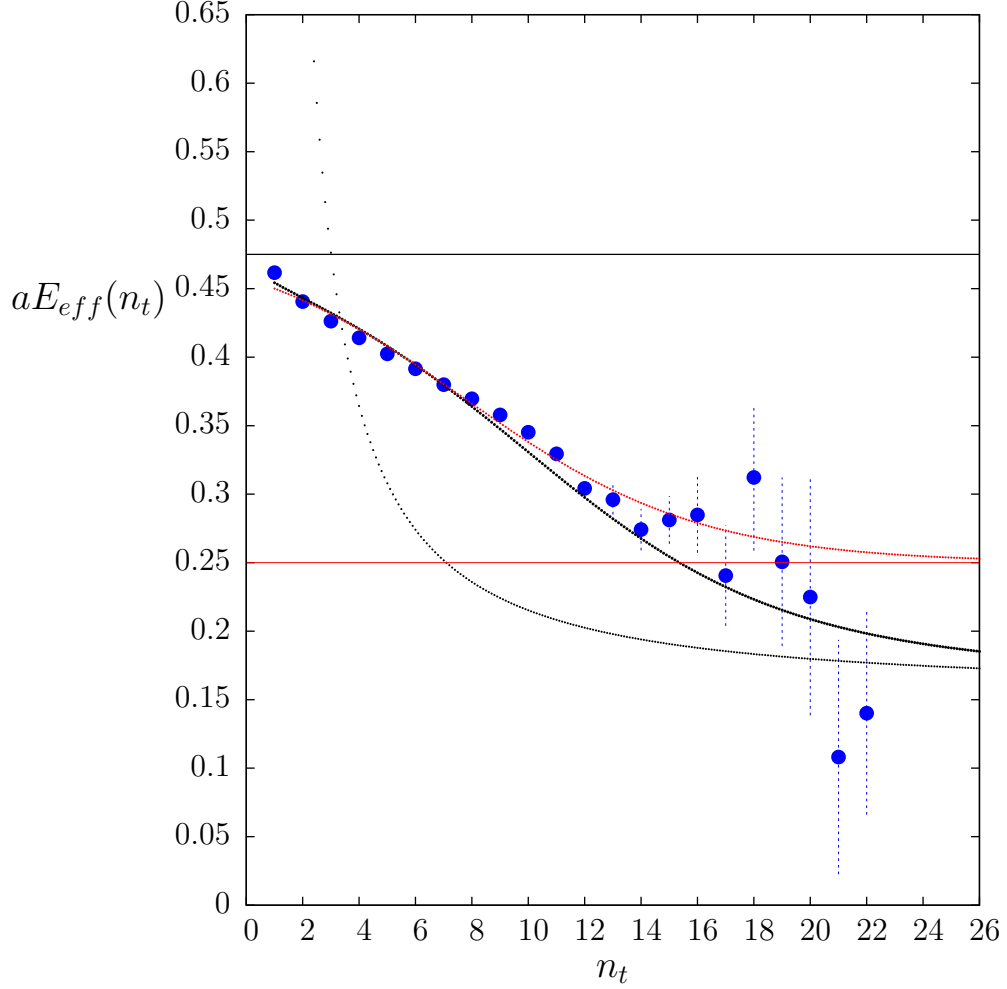


Figure 8: Effective energy, E_{eff} , of the $k=2A$, $p=0$, $P=+$ (variational) first excited state of a flux tube of length $l = 16a$. The red curve is what one obtains with an excited state, $aE^* = 0.49$, in addition to the ground state, which is indicated by the lower horizontal line. The solid black curve is obtained by summing over scattering states of 2 fundamental flux tubes with a Breit-Wigner amplitude peaking at the upper horizontal line and with a width $a\Gamma = 0.065$. The lower black curve sums uniformly over all scattering states.

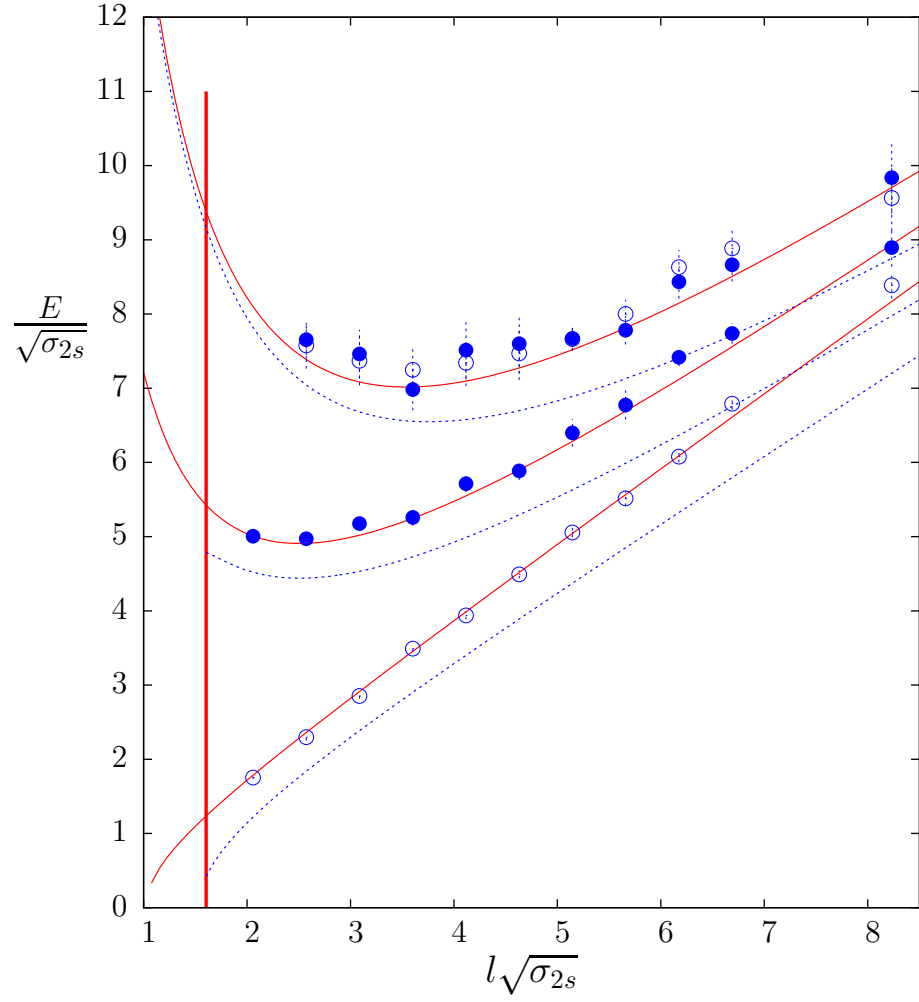


Figure 9: $k = 2S$ ground states with $p = 0, 2\pi/l, 4\pi/l$ and with $P = +$, \circ , and $P = -$, \bullet . Curves are Nambu-Goto predictions. Dashed lines are thresholds for scattering states formed of two fundamental flux tubes with total momentum p . Vertical line denotes location of ‘deconfinement’ transition.

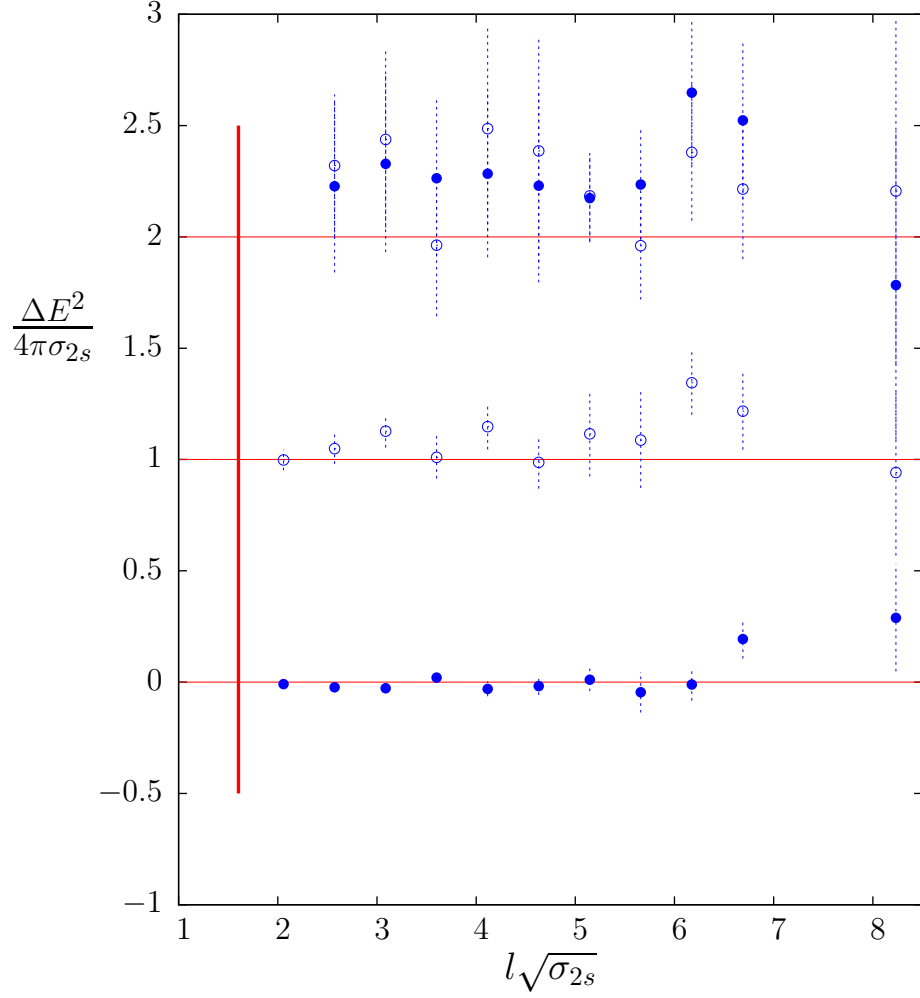


Figure 10: Phonon excitation energies (see eqn(14)) of lowest $k = 2S$ states with $p = 0$ and $P = +, \bullet$, $p = 2\pi/l$ and $P = -, \circ$, and with $p = 4\pi/l$ for both $P = -, \circ$ and $P = +, \bullet$. Horizontal lines are Nambu-Goto predictions. Vertical line denotes location of ‘deconfinement’ transition.

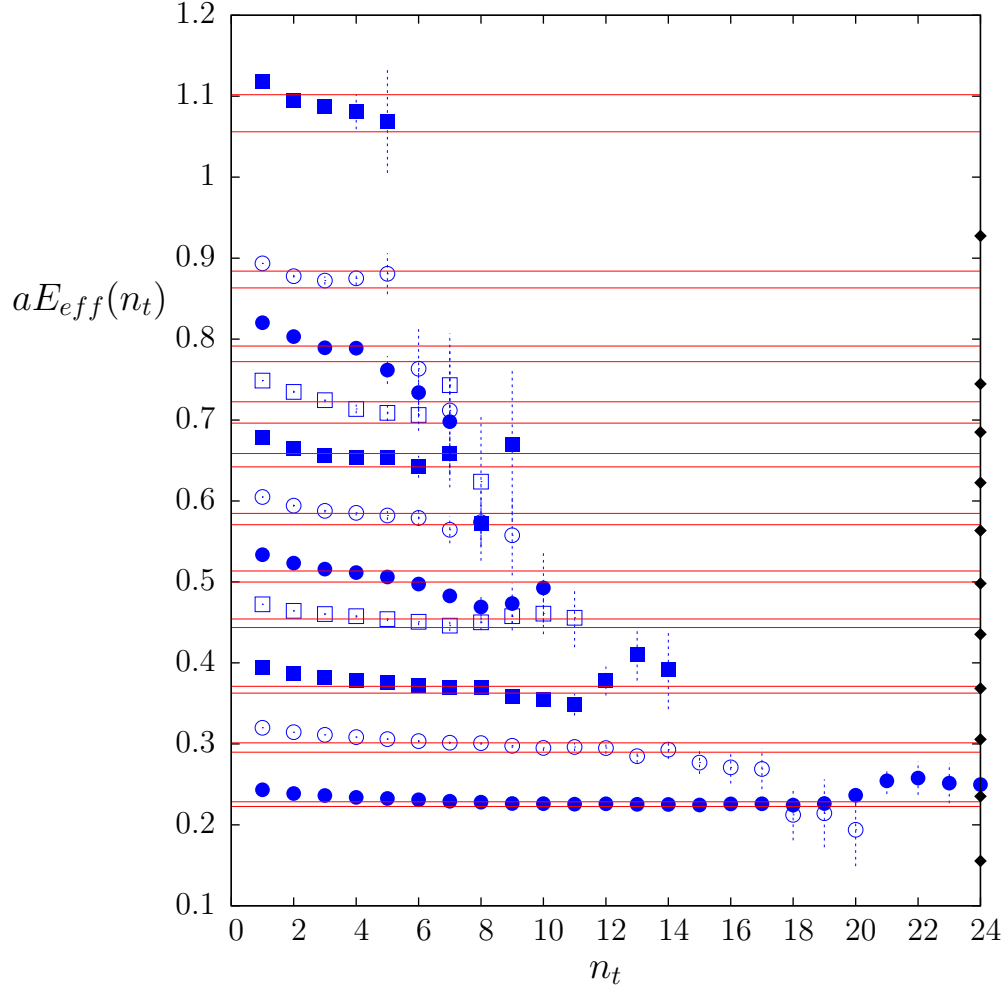


Figure 11: Effective energy of the $k=2S$, $p=0$, $P=+$ (variational) ground state of a flux tube of length $l/a = 16, 20, 24, 28, 32, 36, 40, 44, 48, 52, 64$. Plateau estimate ($\pm 1\sigma$ error band) given by red lines. Lowest energy of two fundamental lines is indicated by diamonds on right axis.

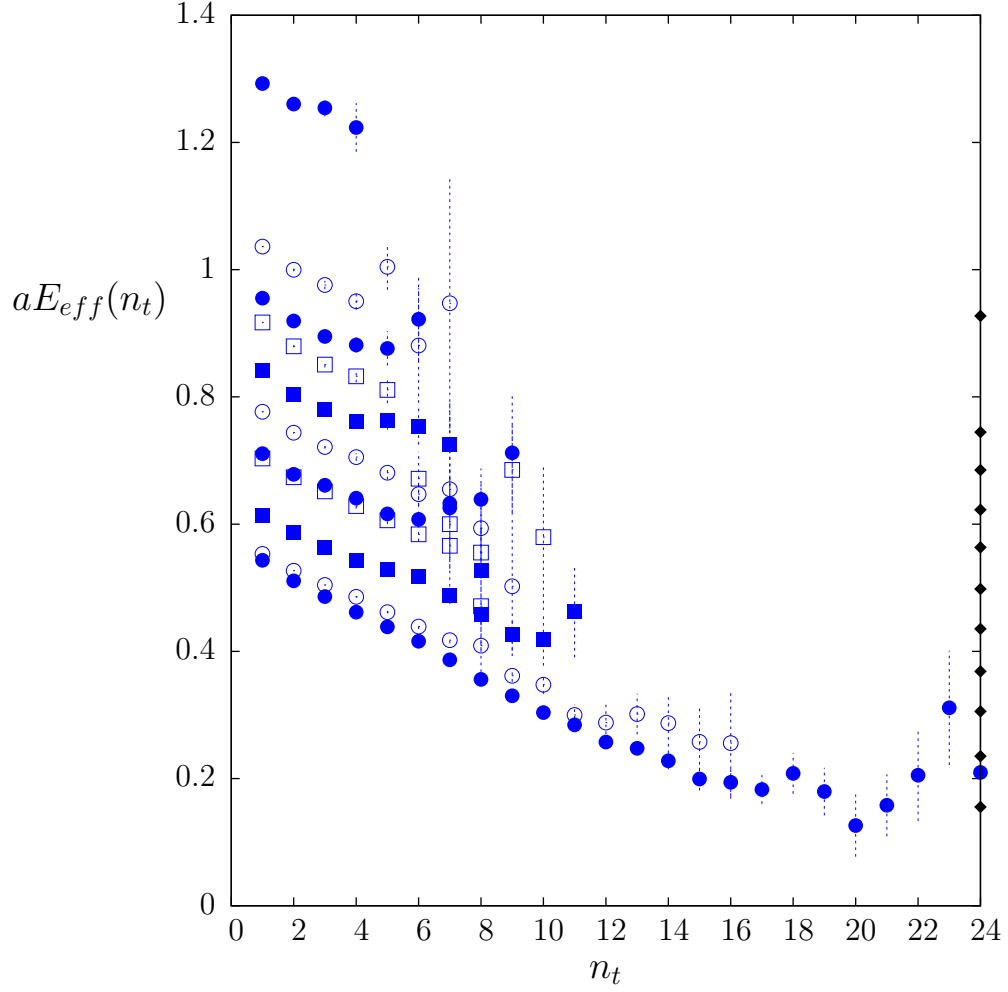


Figure 12: Effective energy of the $k=2S$, $p=0$, $P=+$ (variational) first excited state of a flux tube of length $l/a = 16, 20, 24, 28, 32, 36, 40, 44, 48, 52, 64$. Lowest energy of two fundamental lines is indicated by diamonds on right vertical axis.

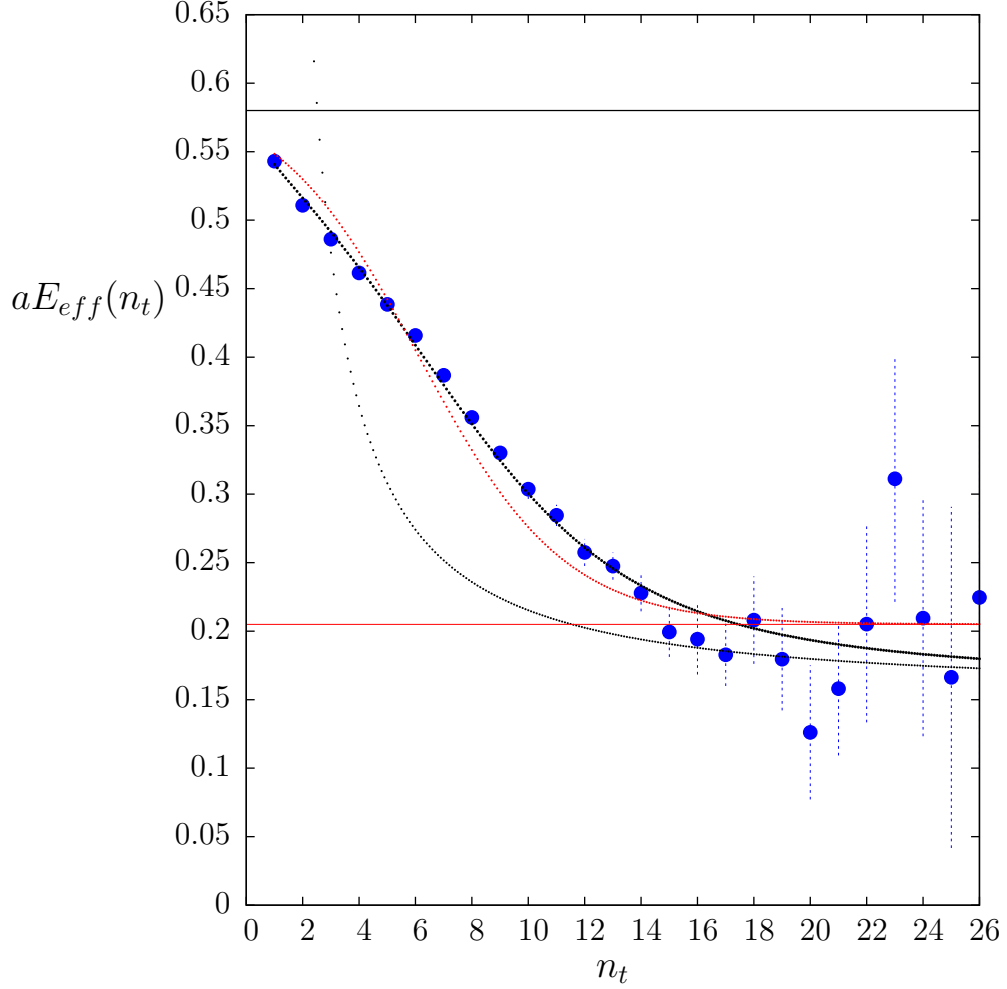


Figure 13: Effective energy, E_{eff} , of the $k=2S$, $p=0$, $P=+$ (variational) first excited state of a flux tube of length $l = 16a$. The red curve is an example of fitting with an excited state, $aE^* = 0.595$, in addition to the ground state indicated by the lower horizontal solid line. The upper black curve is obtained by summing over scattering states of 2 fundamental flux tubes with a Breit-Wigner probability peaking at the upper horizontal line, with width $a\Gamma = 0.12$. The lower black curve sums uniformly over all scattering states.

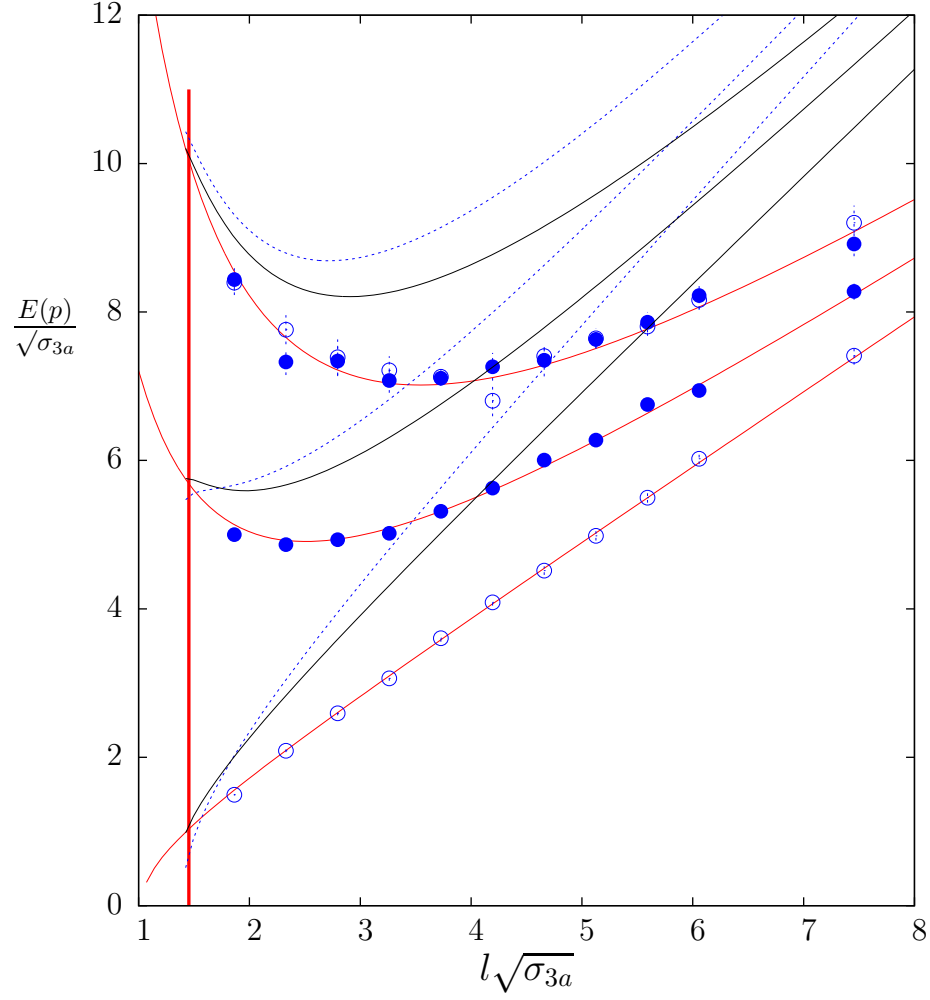


Figure 14: $k = 3A$ ground states with $p = 0, 2\pi/l, 4\pi/l$ and with $P = +, o$, and $P = -, \bullet$. Red curves are Nambu-Goto predictions. Black dashed line denotes lower boundary of scattering state formed of three fundamental flux tubes with total momentum p , and black solid line of a $k = 2A$ flux tube with a fundamental flux tube with total momentum p . Vertical line denotes location of ‘deconfinement’ transition.

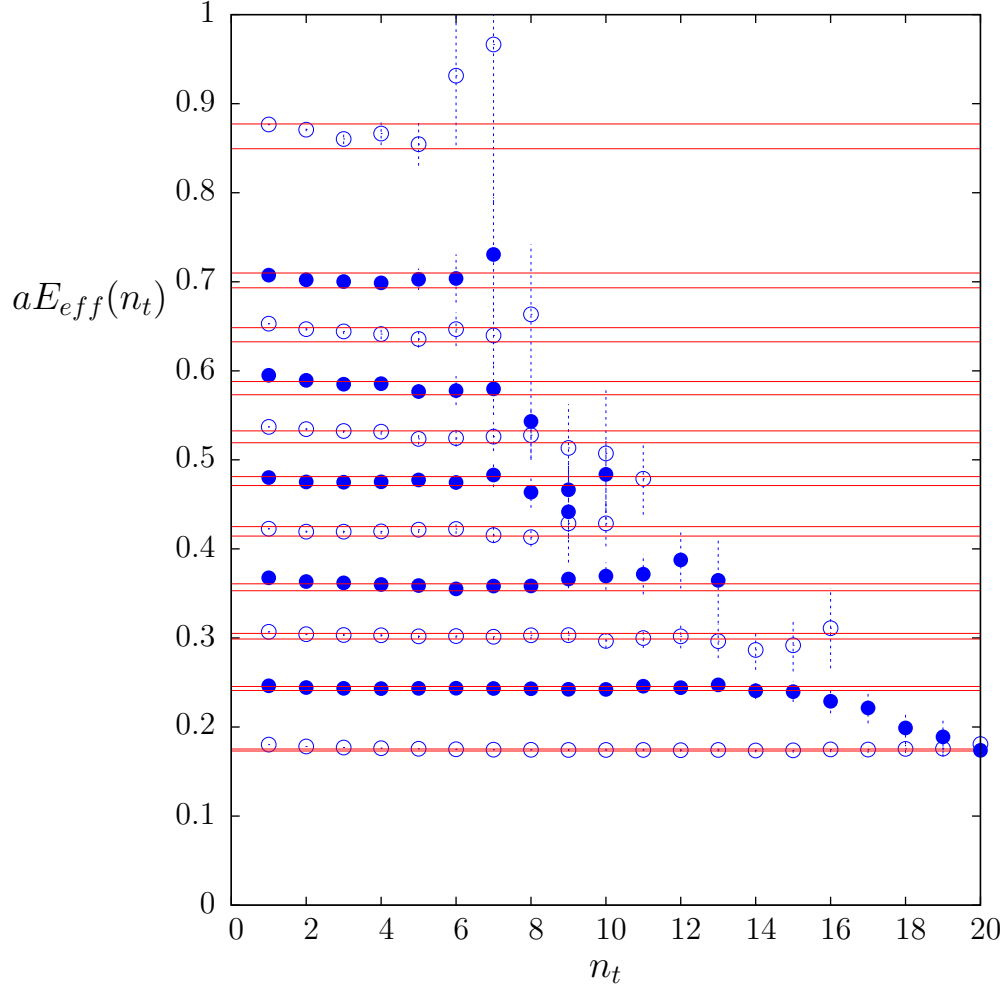


Figure 15: Effective energy of the $k=3A$, $p=0$, $P=+$ (variational) ground state of a flux tube of length $l/a = 16, 20, 24, 28, 32, 36, 40, 44, 48, 52, 64$. Lines are our plateaux estimates ($\pm 1\sigma$ error bands).

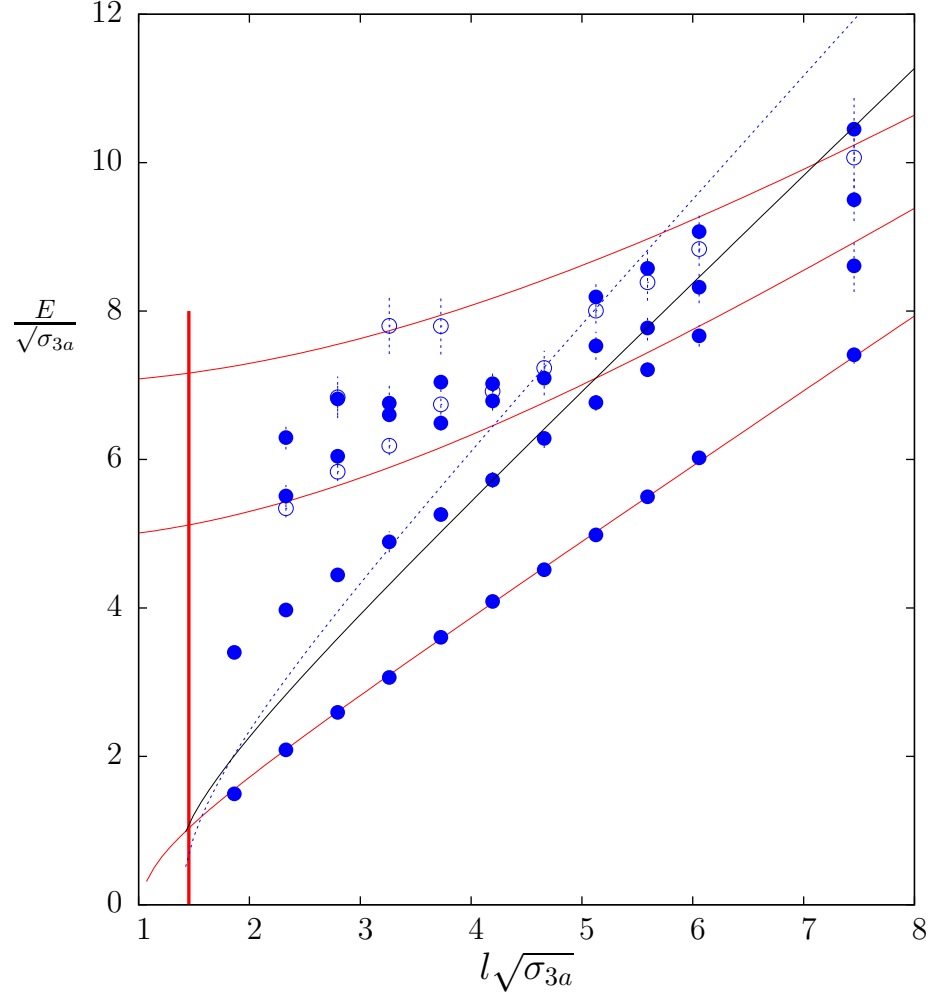


Figure 16: Energies of lightest $k = 3A$ states with $p = 0$ and with $P = +$, \bullet , or $P = -$, \circ . Red curves are corresponding Nambu-Goto levels. Black dashed line is the lowest energy of three fundamental flux loops; solid black line is that of a $k = 2A$ flux tube with a fundamental one. Vertical line denotes location of ‘deconfinement’ transition.

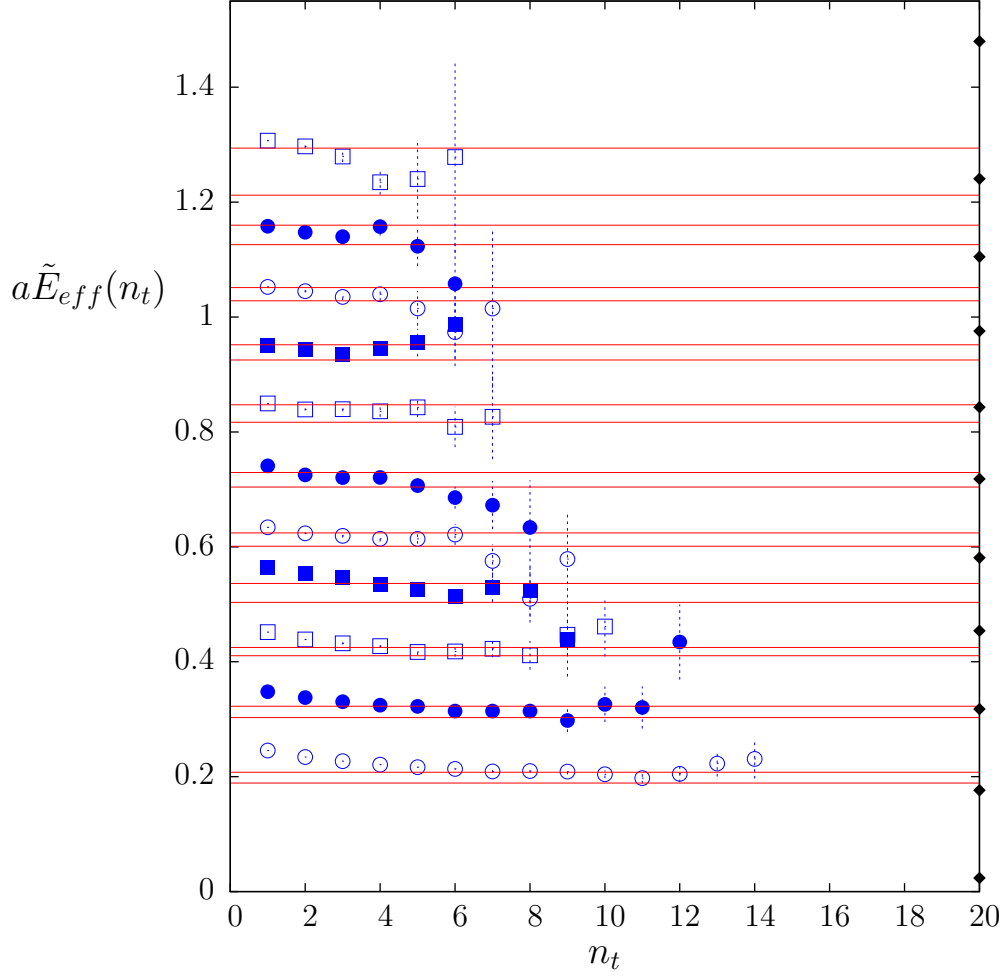


Figure 17: Effective energy, aE_{eff} , of the $k=3A$, $p=0$, $P=+$ (variational) first excited state of a flux tube of length $l/a = 16, 20, 24, 28, 32, 36, 40, 44, 48, 52, 64$. Values shown have been shifted for clarity: $a\tilde{E}_{eff} = aE_{eff} + 0.05 * (l/a - 32)/4$. (Shift of $l = 64a$ is 0.25.) Lines are our plateau estimates ($\pm 1\sigma$ error bands). Thresholds for decay shown as diamonds on right axis.

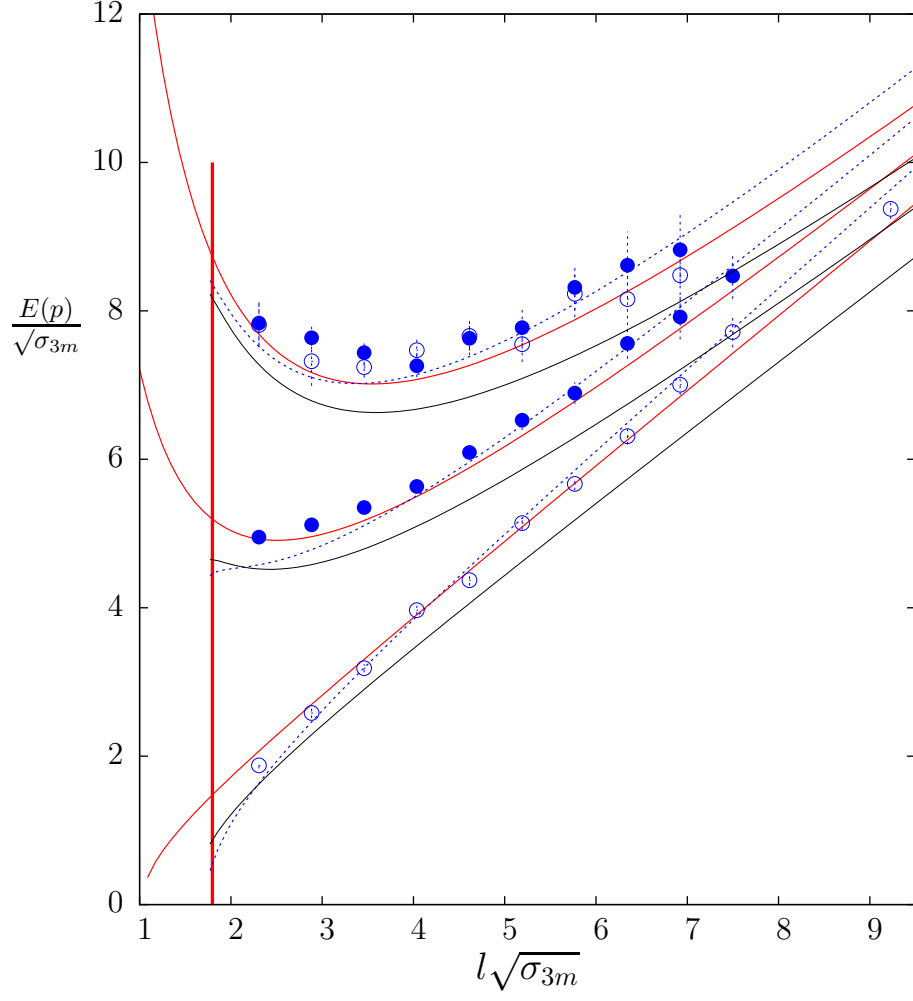


Figure 18: $k = 3M$ ground states with $p = 0, 2\pi/l, 4\pi/l$ and with $P = +, o$, and $P = -, \bullet$. Solid red curves are Nambu-Goto predictions. Dashed line denotes lower boundary of scattering state formed of three fundamental flux tubes with total momentum p ; black line of a $k = 2A$ flux tube with a fundamental flux tube. Vertical line denotes location of ‘deconfinement’ transition.

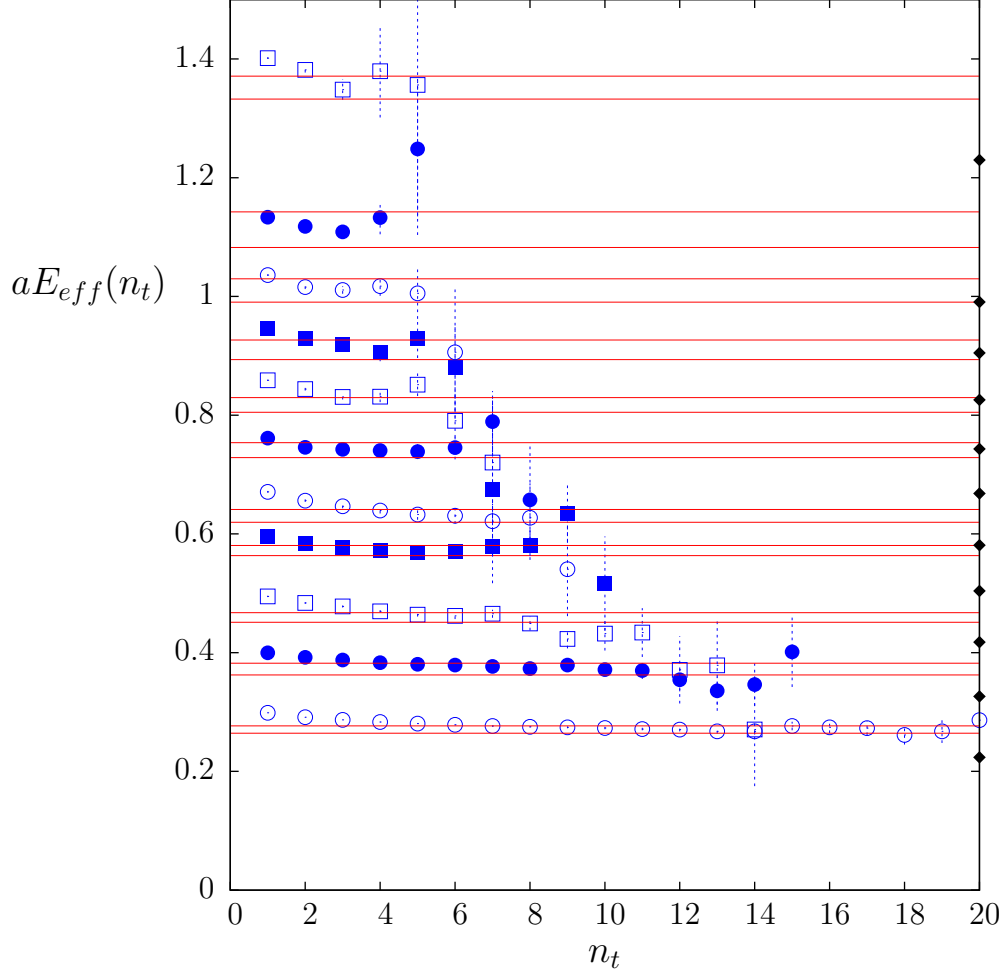


Figure 19: Effective energy of the $k=3M$, $p=0$, $P=+$ (variational) ground state of a flux tube of length $l/a = 16, 20, 24, 28, 32, 36, 40, 44, 48, 52, 64$. Lines are our plateau estimates ($\pm 1\sigma$ error bands). Decay thresholds indicated by diamonds on right axis.

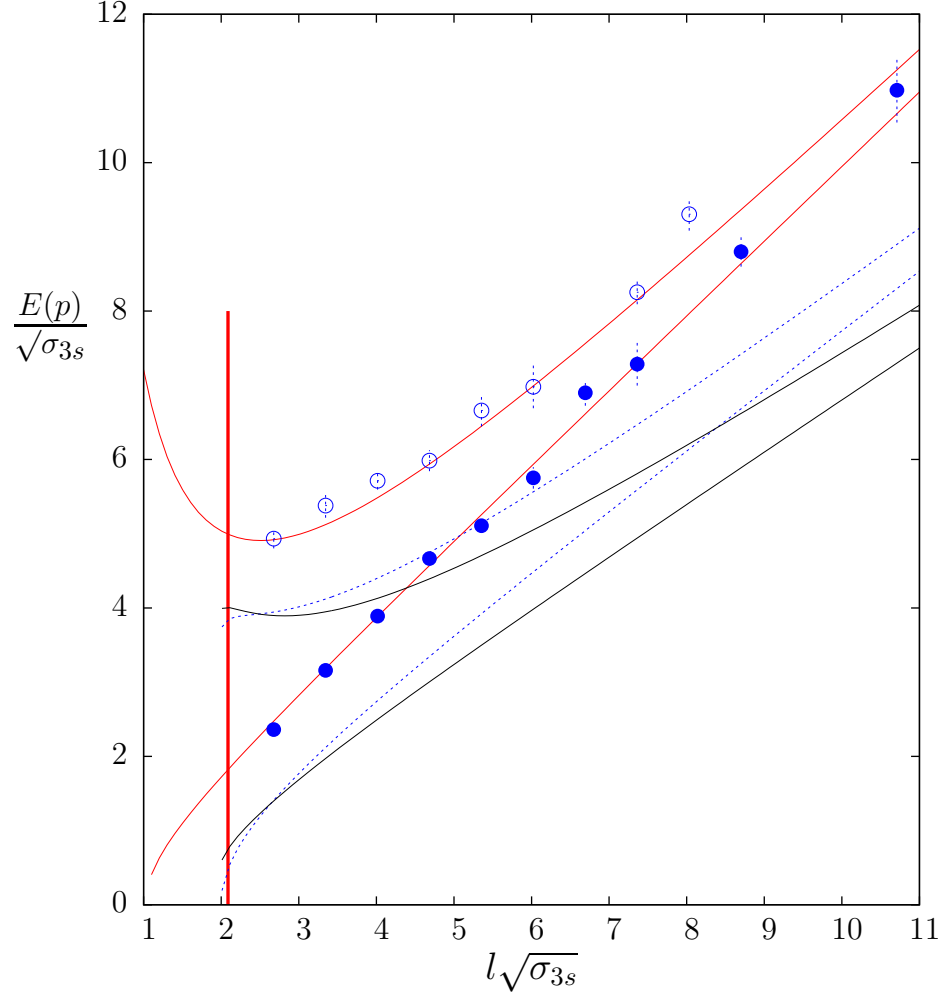


Figure 20: $k = 3S$ ground states with $p = 0, P = +, \bullet$, and with $p = 2\pi/l, P = -, \circ$. Solid red curves are Nambu-Goto predictions. Dashed line denotes lower boundary of scattering state formed of three fundamental flux tubes with same momentum; black line of a $k = 2A$ flux tube with a fundamental flux tube. Vertical line denotes location of ‘deconfinement’ transition.

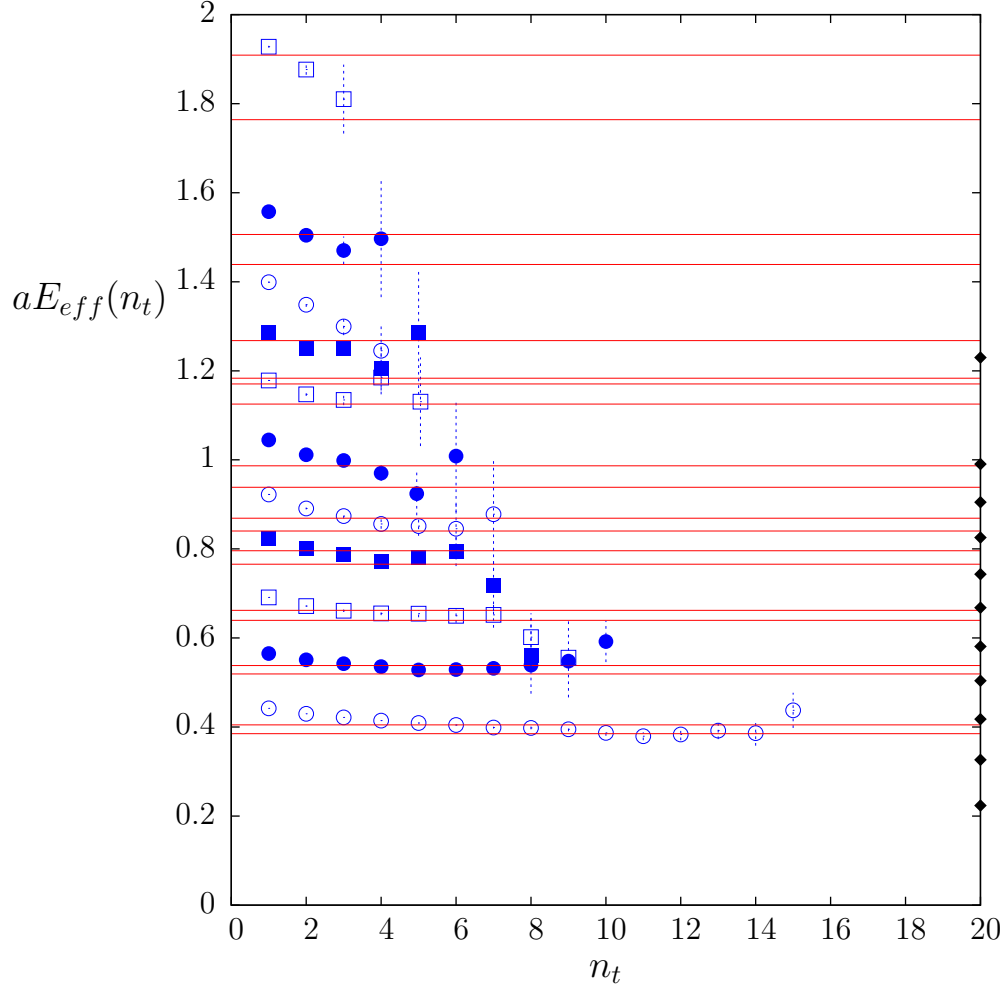


Figure 21: Effective energy of the $k=3S$, $p=0$, $P=+$ (variational) ground state of a flux tube of length $l/a = 16, 20, 24, 28, 32, 36, 40, 44, 48, 52, 64$. Lines are our plateaux estimates ($\pm 1\sigma$ error bands). No plateau attempted for $l = 48a$. Diamonds on right axis denote decay thresholds.

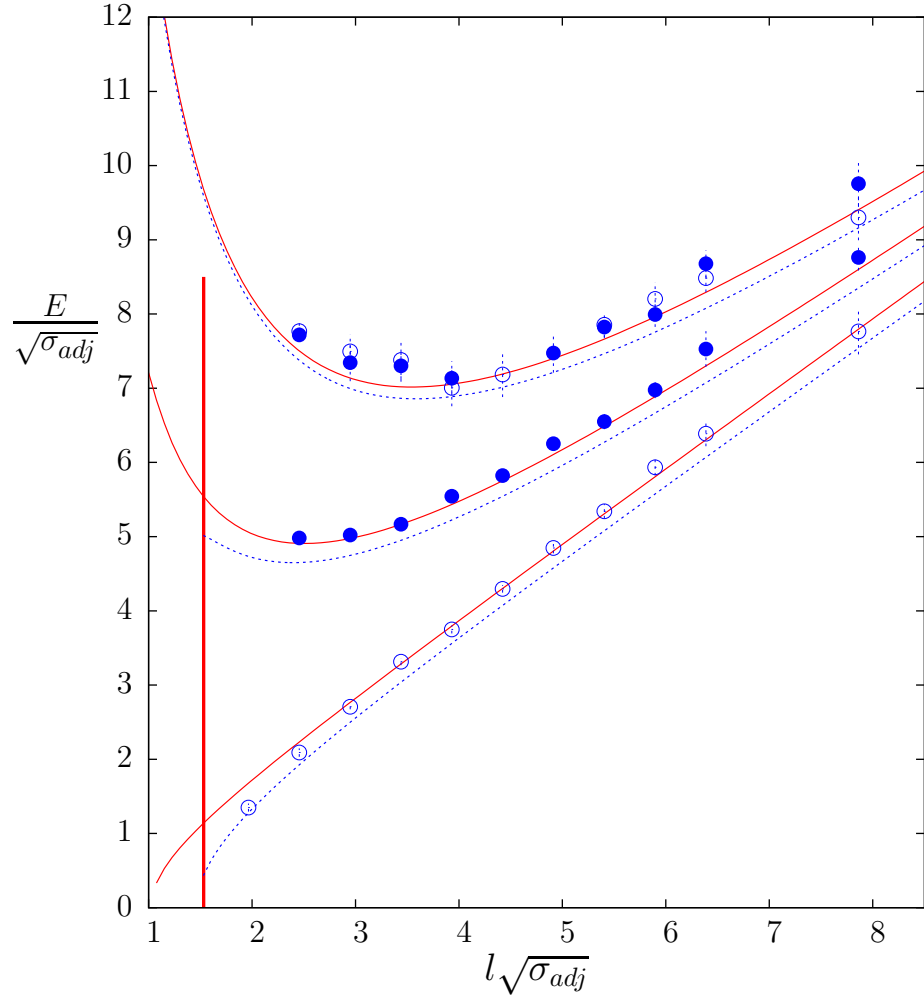


Figure 22: Adjoint ground states with $p = 0, 2\pi/l, 4\pi/l$ and with $P = +, \circ$, and $P = -, \bullet$. Solid red curves are Nambu-Goto predictions. Dashed lines denote lower boundaries of scattering state formed of a pair of (anti)fundamental flux tubes with same momentum. Vertical line denotes location of ‘deconfinement’ transition.

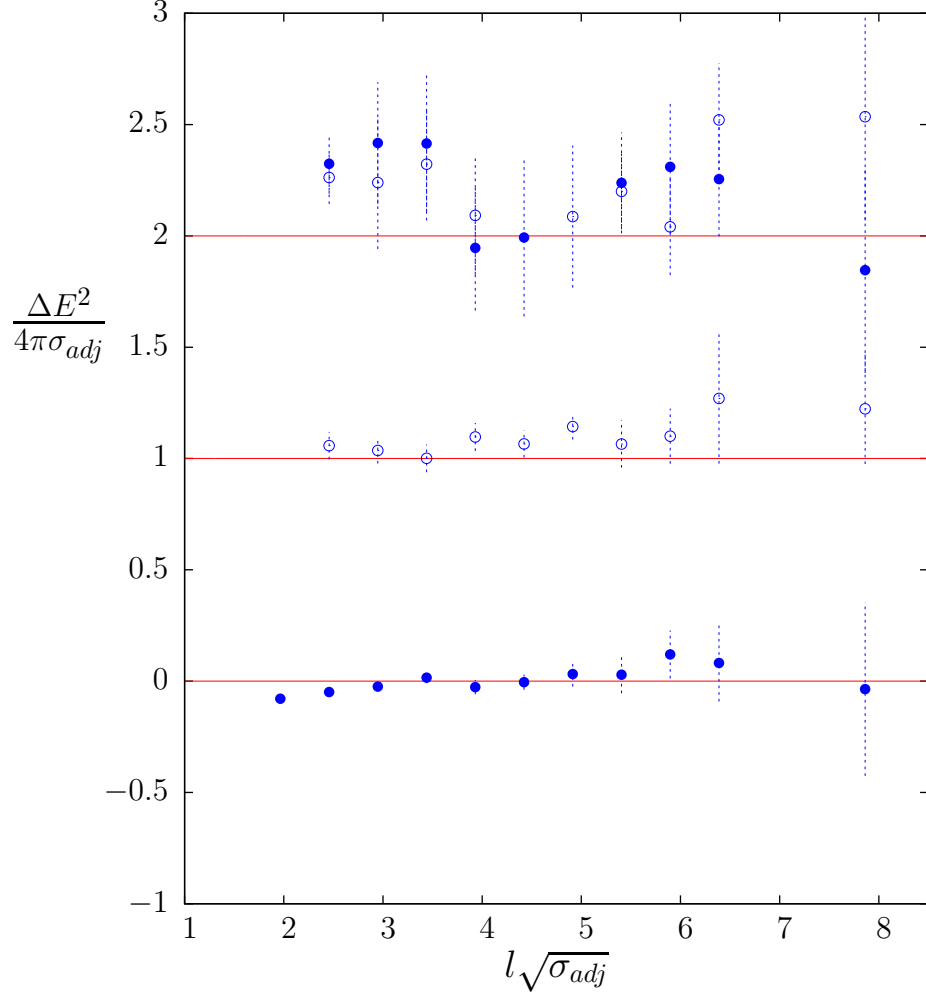


Figure 23: Phonon excitation energies of adjoint ground states with $p = 0$ and $P = +$, ●, $p = 2\pi/l$ and $P = -$, ○, and with $p = 4\pi/l$ for both $P = -$, ◐ and $P = +$, ●. Lines are Nambu-Goto predictions.

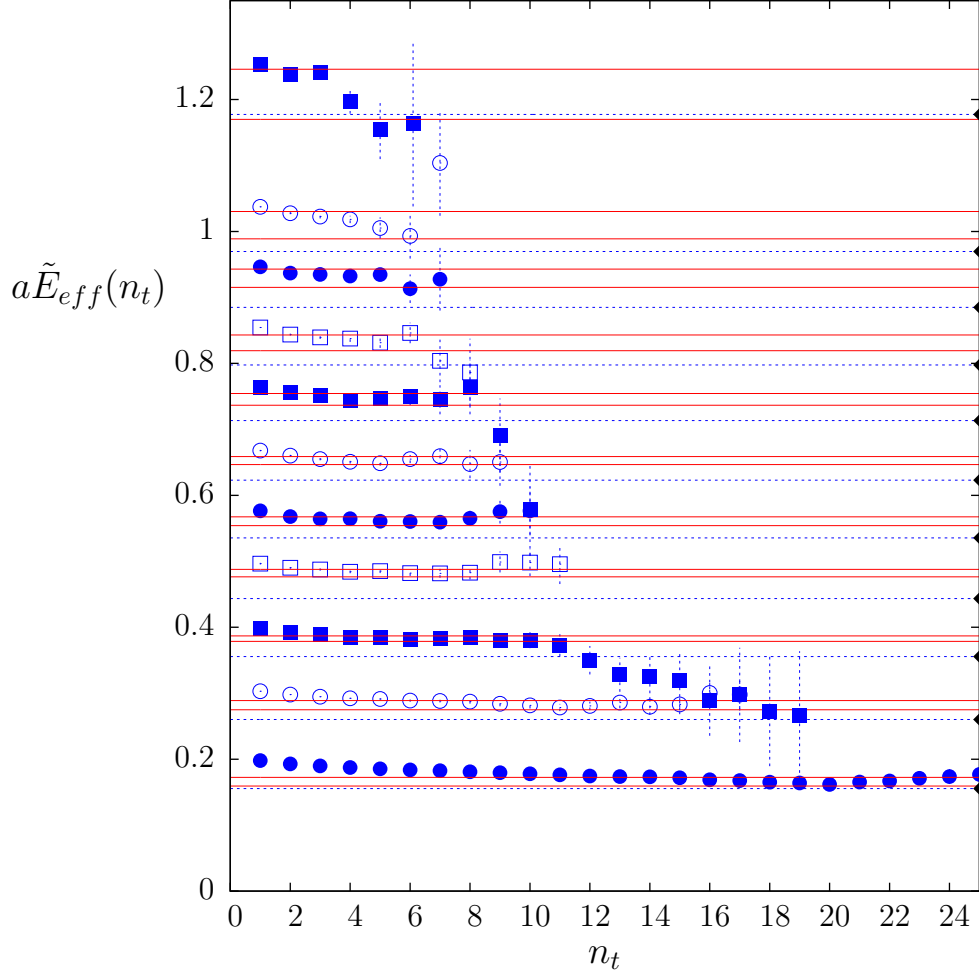


Figure 24: Ground state adjoint loop effective masses for $l/a = 16, 20, 24, 28, 32, 36, 40, 44, 48, 52, 64$. Solid lines give $\pm 1\sigma$ error bands of our plateaux estimates. Dashed lines are twice the energy of corresponding (anti)fundamental loops. (Also indicated by diamonds on right axis.) Values shown have been shifted by multiples of 0.025 for clarity: $a\tilde{E}_{eff} = aE_{eff} + 0.025 * (l/a - 16)/4$, except a shift of 0.25 for $l = 64a$.

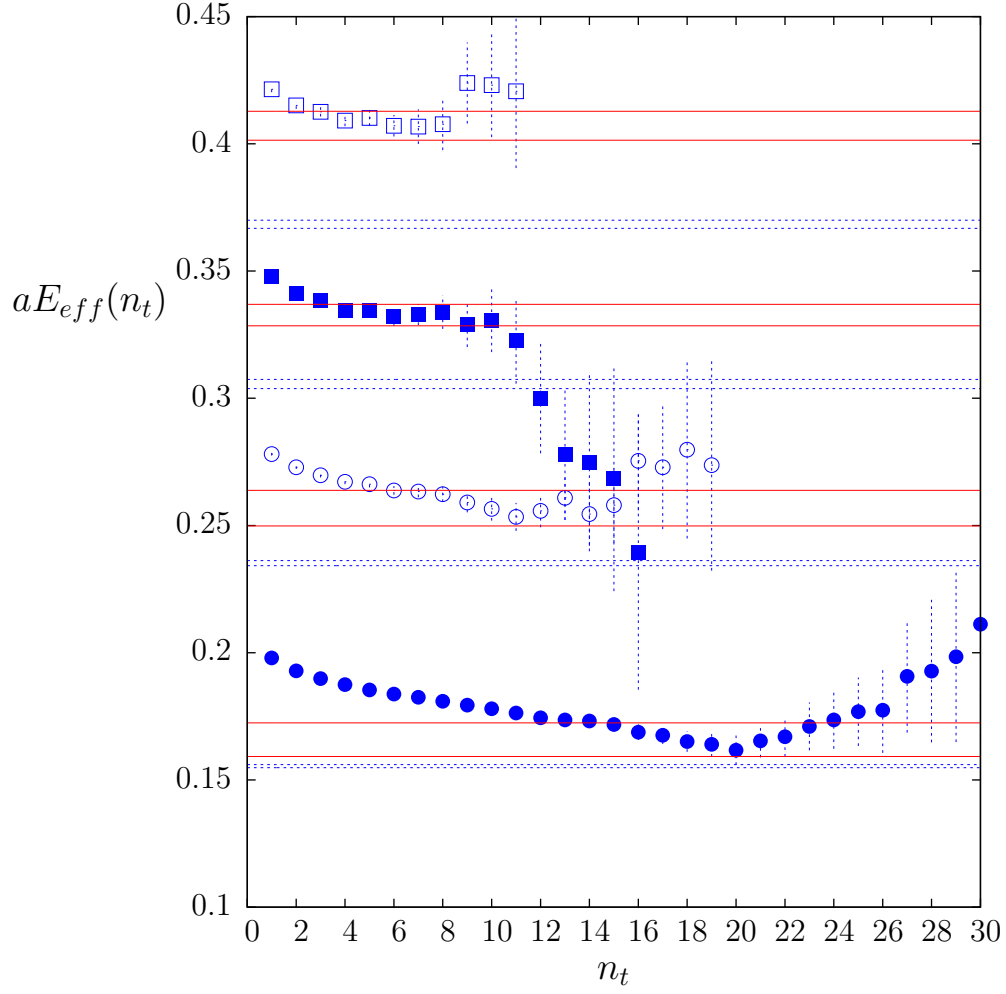


Figure 25: Ground state adjoint loop effective masses for $l/a = 16, 20, 24, 28$. Solid lines give $\pm 1\sigma$ error bands for our plateau estimates. Dashed lines are error bands for twice the energy of corresponding (anti)fundamental loops.

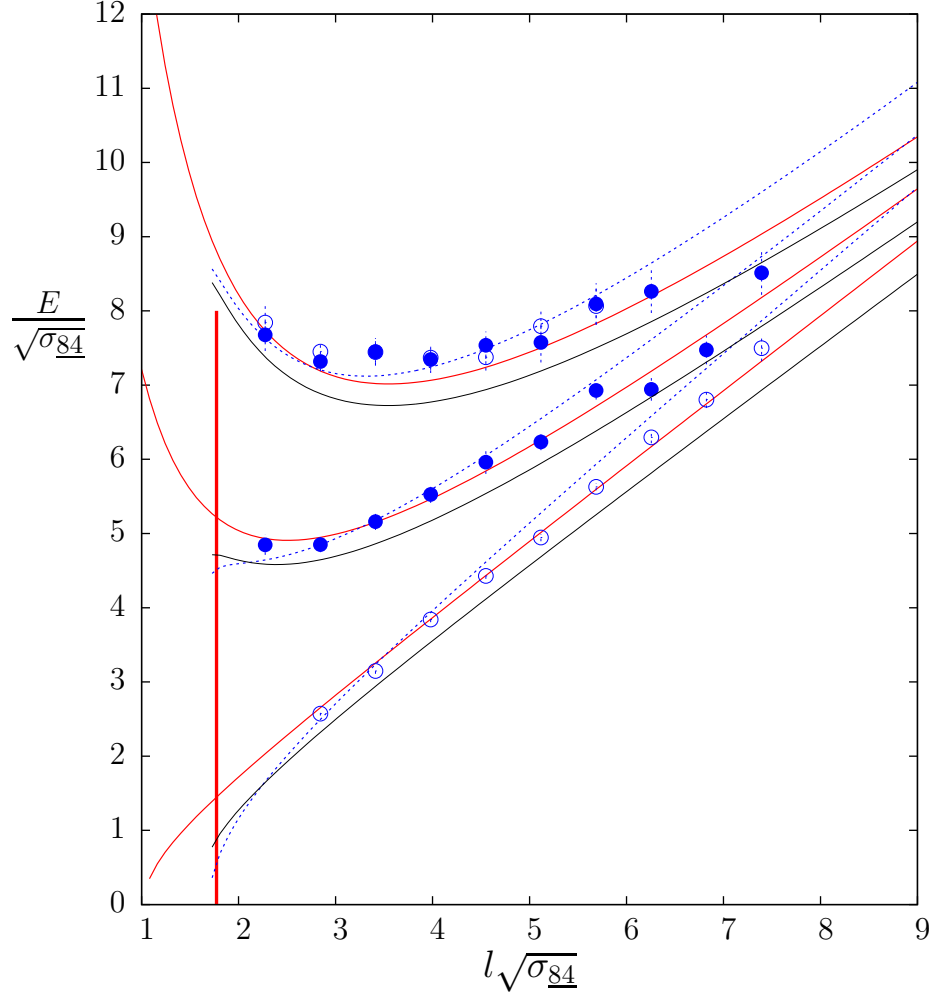


Figure 26: Ground states in the $\underline{84}$ representation for $p = 0, 2\pi/l, 4\pi/l$ and with $P = +$, \circ , and $P = -$, \bullet . Solid red curves are Nambu-Goto predictions. Black dashed line denotes lower boundary of scattering state formed of three (anti)fundamental flux tubes with same momentum, black solid line of one $k = 2A$ and one antifundamental flux tube. Vertical line denotes location of ‘deconfinement’ transition.

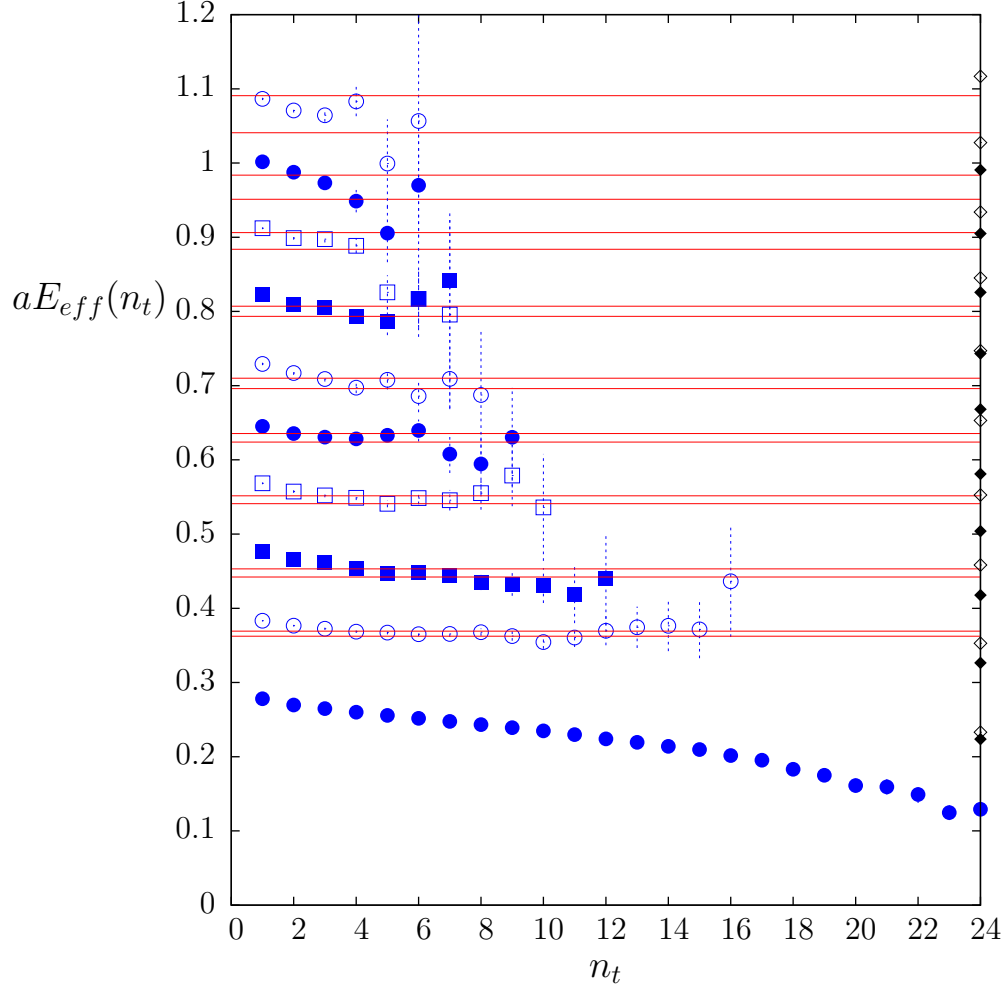


Figure 27: Ground state effective masses of 84 flux tube with $l/a = 16, 20, 24, 28, 32, 36, 40, 44, 48, 52$. Solid lines give error bands of our plateaux estimates. Diamonds on axis indicate $2A + \bar{f}$ (solid) and $f + f + \bar{f}$ (open) decay thresholds.

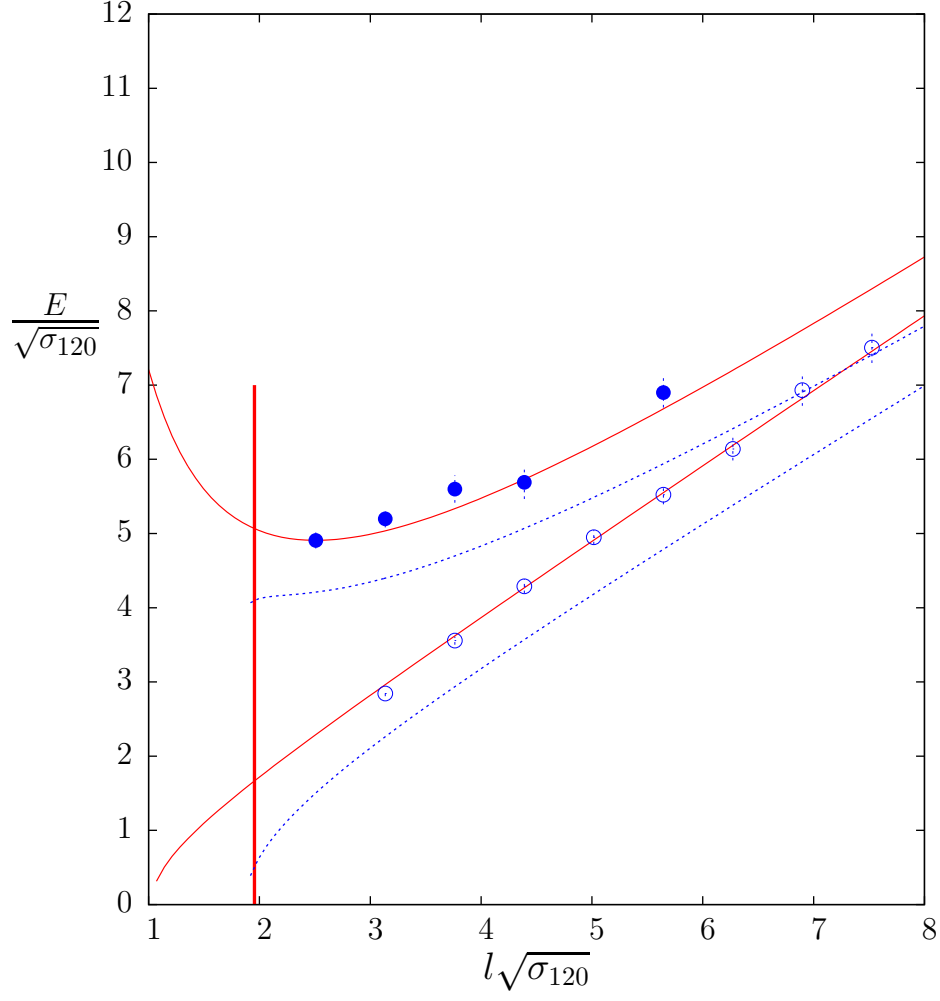


Figure 28: Ground states in the $\underline{120}$ representation for $p = 0, 2\pi/l$ and with $P = +$, \circ , and $P = -$, \bullet . Solid red curves are Nambu-Goto predictions. Black dashed line denotes lower boundary of scattering state formed of three (anti)fundamental flux tubes with same momentum, black solid line of one $k = 2A$ and one antifundamental flux tube. Vertical line denotes location of ‘deconfinement’ transition.

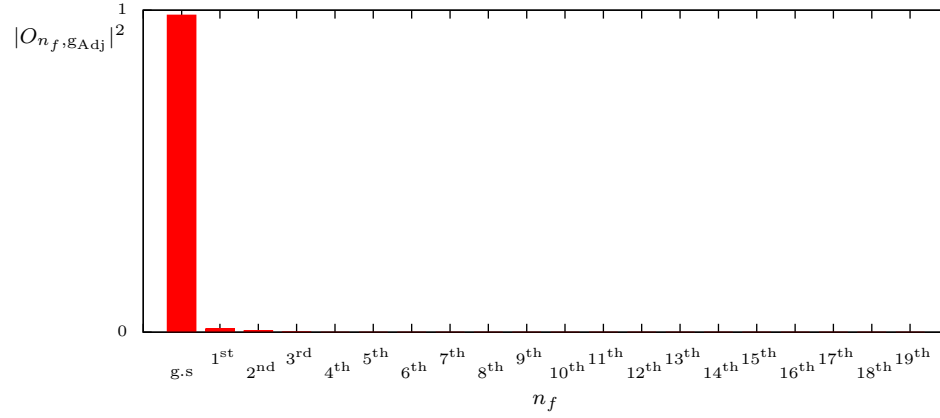
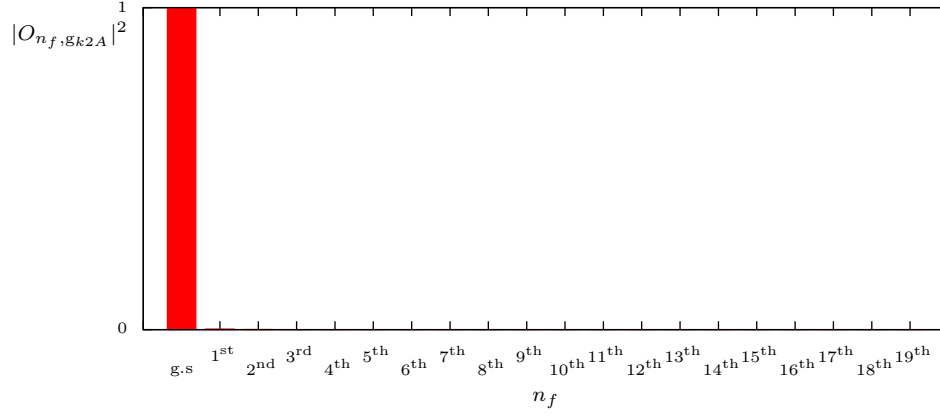


Figure 29: Overlap, as in eqn(21), of $k = 24$ and adjoint ground states onto low-lying fundamental states. For $l = 32a$.

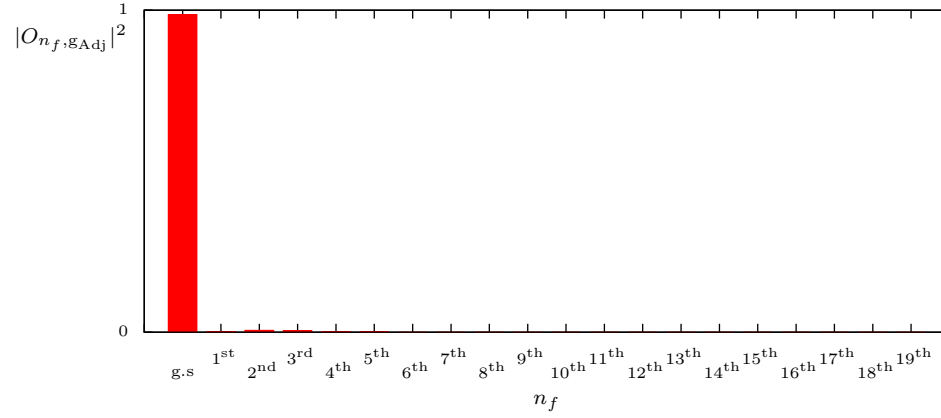
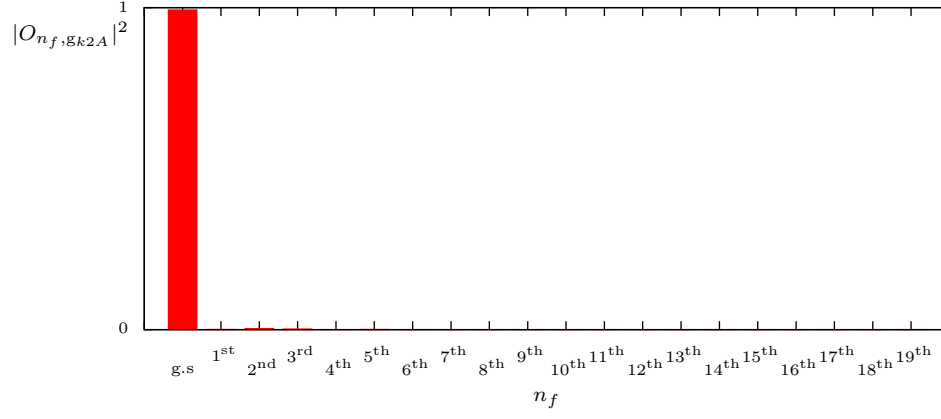


Figure 30: Overlap, as in eqn(21), of $k = 24$ and adjoint ground states onto low-lying fundamental states. For $l = 64a$.

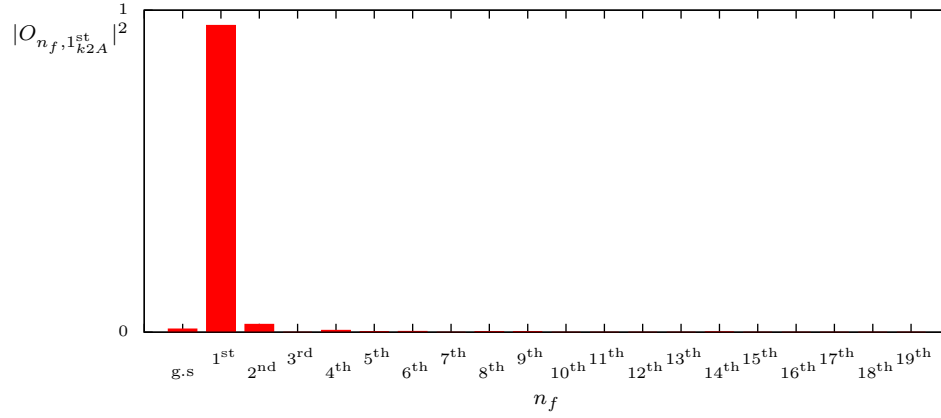
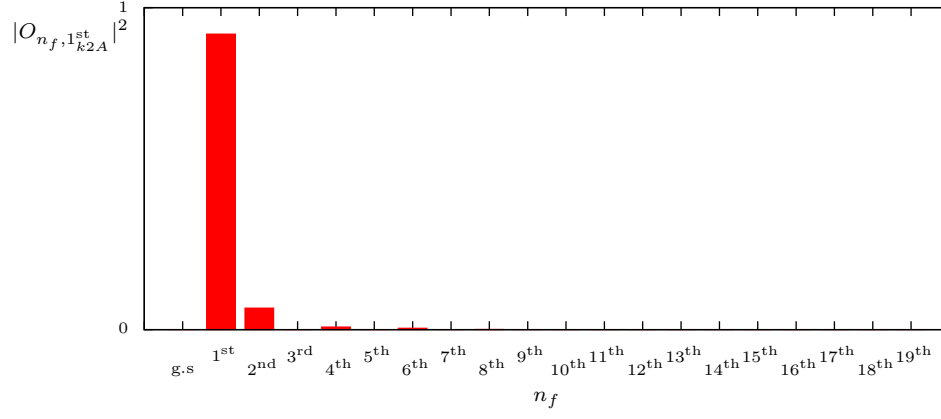


Figure 31: Overlap, as in eqn(21), of $k = 2A$ first excited $p = 0$ state onto low-lying fundamental states. For $l = 32a$ and $l = 64a$.

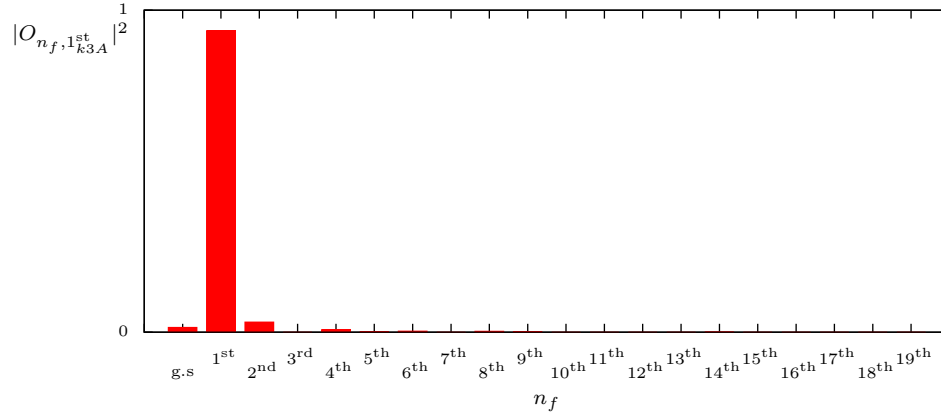
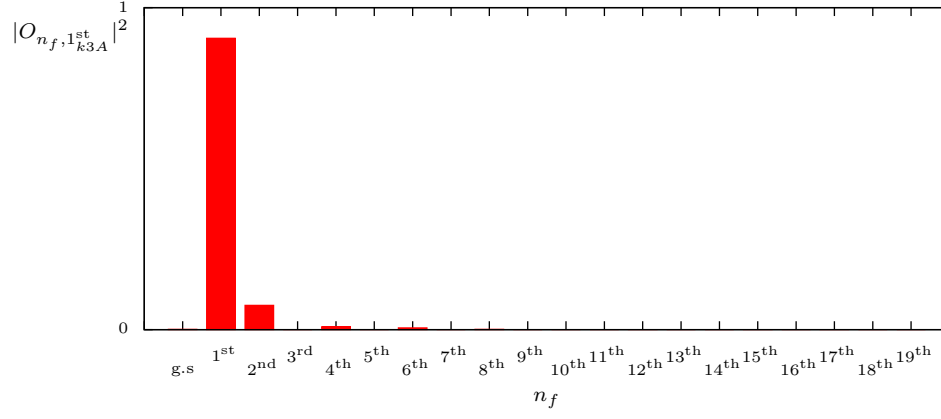


Figure 32: Overlap, as in eqn(21), of $k = 3A$ first excited $p = 0$ state onto low-lying fundamental states. For $l = 32a$ and $l = 64a$.

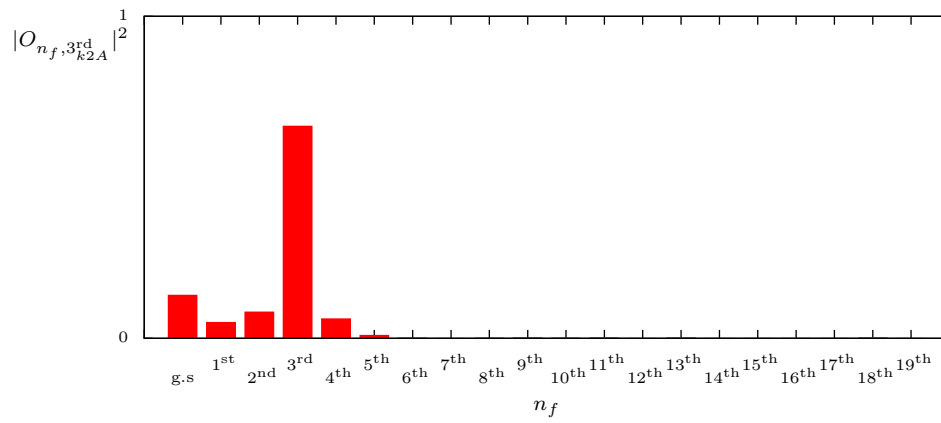
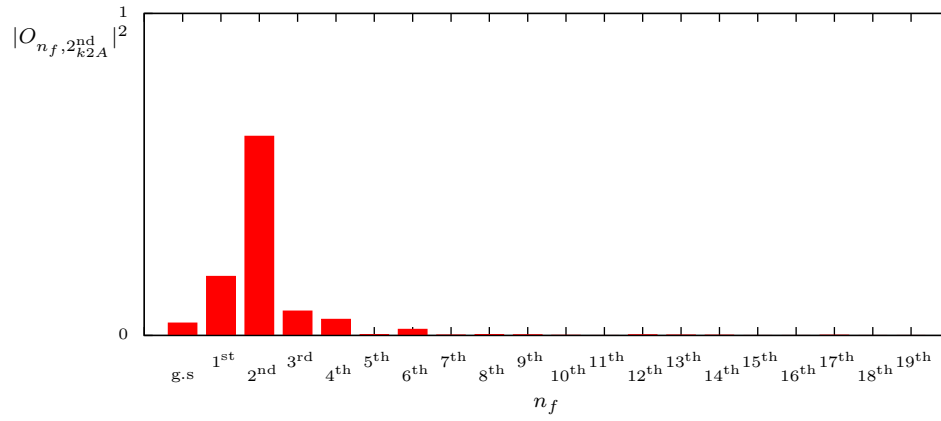


Figure 33: Overlap, as in eqn(21), of $k = 2A$ second and third excited $p = 0$ states onto low-lying fundamental states. For $l = 32a$.

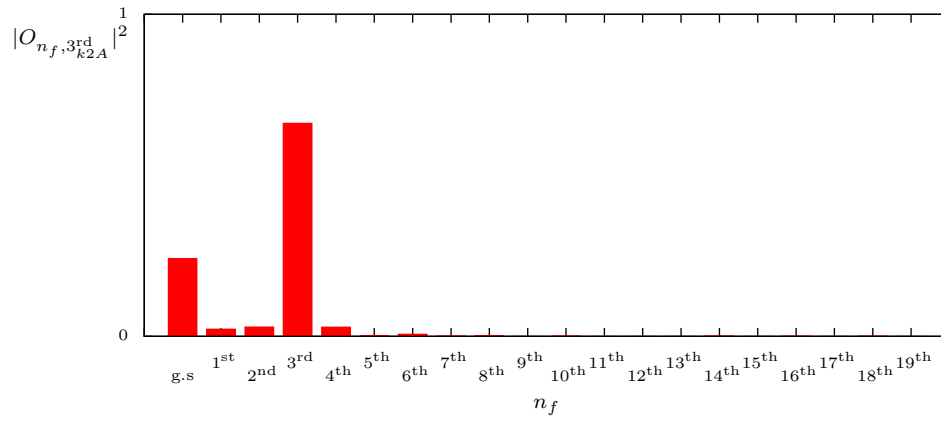
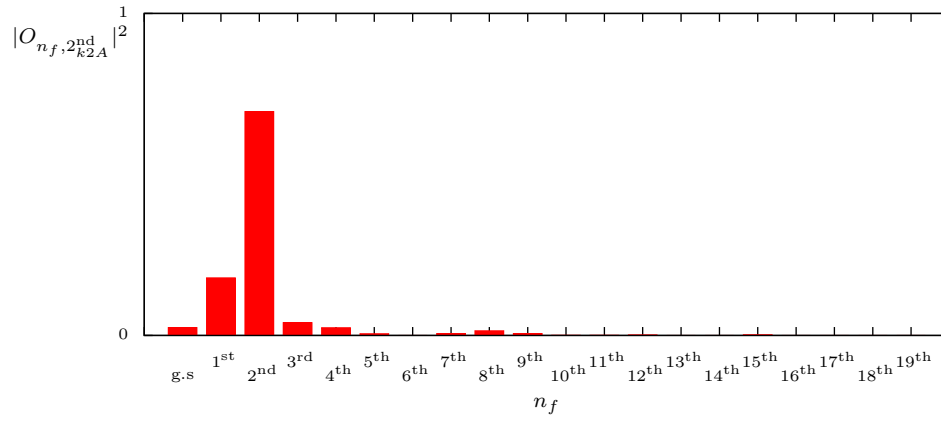


Figure 34: Overlap, as in eqn(21), of $k = 2A$ second and third excited $p = 0$ states onto low-lying fundamental states. For $l = 52a$.